SCIENCE CHINA
Physics, Mechanics & Astronomy

• Invited Review •

May 2020 Vol. 63 No. 5: 250001
https://doi.org/10.1007/s11433-019-1477-7

Holographic topological semimetals

Karl Landsteiner[1*], Yan Liu[2,3*], and Ya-Wen Sun[4,5]

[1] *Instituto de Física Teórica UAM/CSIC, C/ Nicolás Cabrera 13-15, Campus Cantoblanco, Cantoblanco 28049, Spain;*
[2] *Center for Gravitational Physics, Department of Space Science, Beihang University, Beijing 100191, China;*
[3] *Key Laboratory of Space Environment Monitoring and Information Processing, Ministry of Industry and Information Technology, Beijing 100191, China;*
[4] *School of Physics & CAS Center for Excellence in Topological Quantum Computation, University of Chinese Academy of Sciences, Beijing 100049, China;*
[5] *Kavli Institute for Theoretical Sciences, University of Chinese Academy of Sciences, Beijing 100049, China*

Received October 14, 2019; accepted November 8, 2019; published online February 25, 2020

The holographic duality allows to construct and study models of strongly coupled quantum matter via dual gravitational theories. In general such models are characterized by the absence of quasiparticles, hydrodynamic behavior and Planckian dissipation times. One particular interesting class of quantum materials are ungapped topological semimetals which have many interesting properties from Hall transport to topologically protected edge states. We review the application of the holographic duality to this type of quantum matter including the construction of holographic Weyl semimetals, nodal line semimetals, quantum phase transition to trivial states (ungapped and gapped), the holographic dual of Fermi arcs and how new unexpected transport properties, such as Hall viscosities arise. The holographic models promise to lead to new insights into the properties of this type of quantum matter.

gauge/gravity duality, topological semimetal, Weyl semimetal, anomaly

PACS number(s): 11.15.-q, 04.62.+v, 11.30.Rd, 03.65.Vf, 67.55.Hc

Citation: K. Landsteiner, Y. Liu, and Y.-W. Sun, Holographic topological semimetals, Sci. China-Phys. Mech. Astron. **63**, 250001 (2020), https://doi.org/10.1007/s11433-019-1477-7

Contents

*Corresponding authors (Yan Liu, email: yanliu@buaa.edu.cn; Karl Landsteiner, email: karl.landsteiner@csic.es)

1 Introduction

Weyl semimetals are a very interesting new form of gapless topological quantum matter [1-5]. What makes them special is that the electronic excitations behave in a very unusual way. The electronic quasiparticles can be described by the Weyl equation known from high energy physics. In the massless limit the Dirac equation can be decomposed into two irreducible parts, called Weyl equations which differ by chirality. In this way the electronics of Weyl semimetals is governed by the laws of relativistic physics. One of the cornerstones of relativistic quantum field theory is that the concept of chirality is sometimes incompatible with quantum theory. Whereas classically the number of left- and right-handed chiral fermions is separately conserved, quantum mechanically this is no longer true. This is the so-called chiral anomaly [6, 7]. Since the electronics of Weyl semimetals is governed by the chiral Weyl equation the chiral anomaly also has profound consequences on the physics of these materials. Many of the most exotic and interesting phenomena such as the the appearance of surface states (Fermi-arcs) or exotic transport phenomena such as the Hall effect are directly linked to the chiral anomaly. Much of the physics of Weyl semimetals can be understood by analyzing the properties of the one-particle wave function. For example the anomaly can be understood as the effect of non-vanishing Berry flux through the Fermi surface, and chirality manifests itself as monopole like singularity of the Berry connection [8]. These notions are of course bound to the validity of a quasiparticle picture in which interactions play a subordinate role. The question arises then if the salient features of Weyl semimetals do persist in a strong coupling context in which there are no clear quasiparticle excitations.

The holographic duality (also known as AdS/CFT correspondence and gauge/gravity duality) has been used over the last decade and a half as a tool to investigate precisely this type of questions. No attempt will be made here to give a concise account of the workings of the holographic duality. There are excellent reviews available in refs. [9-13]. In fact the holographic duality has provided already outstanding results. The modern understanding of hydrodynamics as a derivative expansion and its validity is put to an all new and sound footing using insights from holography [14, 15]. Anomaly induced transport properties [16, 17] such as the chiral magnetic and chiral vortical effects and their relations to anomalies can be most easily understood with the means of holographic duality [18, 19]. The reader is reminded of the conceptual difficulties in the interpretation of the formula for chiral magnetic effect. This is in sharp contrast with the clarity of its theory in holography. It is by now well-known

that the chiral magnetic effect vanishes in equilibrium but it is probably not universally acknowledged that this has been calculated first in holographic models [20]. Another example is the direct connection between the temperature dependence of the chiral vortical effect and the gravitational contribution to the chiral anomaly [21,22]. Therefore holographic duality is not only interesting because of its inherently strongly coupled nature but also because it gives valuable insight via the holographic perspective on conceptually difficult problems such as anomaly induced transport. This provides more than sufficient theoretical motivation for studying holographic models of Weyl semimetals. It is also noteworthy that hydrodynamics and thus strongly coupling behavior has been reported for the Weyl semimetal WP_2 [23]. It is possible that holographic models can serve as models for such type of materials. As we will review here, also in the case of Weyl semimetals holography is able to provide new perspectives, leading to new directions of research and even allowing the discovery of new, possibly unexpected transport phenomena.

The review is organized as follows. In sect. 2 we give a flash review of the holographic duality. Then we introduce the holographic model of a (time reversal symmetry breaking) Weyl semimetal in sect. 3. The most important results stemming from working with this model are also reviewed. These include the existence of a quantum phase transition between the Weyl semimetal and a topological trivial state, calculation of the Hall conductivity, the calculation of topological invariants via fermionic holographic spectral functions, finite temperature and viscosities, in particular the appearance of Hall viscosity at the critical point of the quantum phase transition, the calculation of the axial Hall conductivity, the effects of disorder and the properties of quantum chaos across the quantum phase transition.

All these results are obtained in models that show a transition between the Weyl semimetal and a trivial semimetal. In sect. 4 a new model is introduced in which the transition is between the Weyl semimetal and an insulating state. In sect. 5 a generalization to holographic nodal line semimetals is discussed. We briefly point to alternative approaches of applications of the holographic duality to the physics of Weyl semimetals in sect. 6. In sect. 7 we first briefly summarize and then give an outlook on possible interesting future directions of research.

2 A short review on the holographic duality

We now give a flash review on the holographic duality [9-12]. The origin of the holographic duality lies in string theory. In its original form it states that a certain type of string theory (type IIB) on the space $AdS_5 \times S^5$ is dual to $N = 4$ supersymmetric gauge theory with gauge group $SU(N_c)$ in four dimensions [24]. String theory needs ten dimensions and that is why there is the compact five sphere. The isometry group of this five dimensional sphere is SO(6). In the dual field theory this is the internal global symmetry of the $N = 4$ gauge theory. The metric of the five dimensional anti de-Sitter (AdS) space is

$$ds^2 = \frac{r^2}{L^2}\left(-dt^2 + d\mathbf{x}^2\right) + \frac{L^2}{r^2}dr^2, \tag{1}$$

where $1/L^2$ is a measure for the curvature of the AdS space.

The $N = 4$ supersymmetric gauge theory with gauge group $SU(N_c)$ in four dimensions is characterized by two physical parameters the Yang-Mills coupling g_{YM} and the rank N_c of $SU(N_c)$. On the dual string theory side, there are two parameters, the fundamental length scale l_s and the string coupling g_s (the amplitude for a string to split in two). The AdS_5 geometry has curvature $R = -20/L^2$ where L is an AdS radius scale. These parameters are related in the AdS/CFT correspondence as the following way:

$$g_{YM}^2 N_c \propto \frac{L^4}{l_s^4}, \tag{2}$$

$$1/N_c \propto g_s. \tag{3}$$

From the above relations, we can see that the AdS/CFT correspondence is a strong weak duality. From eq. (2), for weak curvature on the string theory side the AdS radius L is large which indicates a large 't-Hooft coupling constant on the field theory. In this parameter regime we can neglect the stringy effects and use type IIB supergravity to approximate the string theory. If we further take the rank N_c of the gauge group to be very large, i.e., the large N_c limit, for the string theory g_s is very small, we can ignore the quantum loop effects and end up with the theory of classcal supergravity!

From the above analysis, we found that the classical (super-)gravity on AdS_{d+1} space is the infinite coupling and infinite rank limit of a gauge theory in d dimensions. This is known as the AdS/CFT correspondence in its most useful form for applications to quantum many body physics. Here we have allowed ourselves to be already a bit more general. Once we have understood the original example based on the maximally supersymmetric four dimensional field theory, we conjecture that every gravitational theory with some additional suitably chosen matter fields on AdS_{d+1} is dual to a certain d dimensional quantum field theory. We take this point of view in the applications of the AdS/CFT correspondence to quantum many body systems. The additional matter fields chosen on the gravity side is according to a particular symmetric property of the underlying quantum field theoretical system that one is interested in.

The dual field theory lives in the four dimensional spacetime parametrized by $(t, \mathbf{x})$, where $\mathbf{x}$ denotes the vector of spatial coordinates (x, y, z). It is sometimes said that the dual field theory lives on the the boundary of AdS space when taking the limit $r \to \infty$. But this is not really true, all of the bulk has a field theory interpretation. The best way of thinking about the "holographic" direction is as an energy scale. The high energy limit of the theory is given by $r \to \infty$ and vice versa the infrared limit is $r \to 0$. This allows a direct geometric interpretation of the renormalization group flow of a holographic theory from the ultraviolet (UV) to the infrared (IR).

The other important ingredient of the holographic dictionary, the rules that allow us to extract field theory information from gravitational physics is the identification between fields in AdS and operators and couplings of the dual field theory. If we consider the solution to a (second-order) field equation in AdS space it allows an expansion for large r of the form:

$$\Phi = \frac{1}{r^{\Delta_-}}\left(\Phi_0(x) + O\left(\frac{1}{r^2}\right)\right) + \frac{1}{r^{\Delta_+}}\left(\Phi_1(x) + O\left(\frac{1}{r^2}\right)\right). \tag{4}$$

We assume there that $\Delta_\pm \geq 0$ and $\Delta_- < \Delta_+$. $\Phi_0(x)$ is the boundary value (non-normalizable mode) of the field $\Phi(r, x)$ in AdS space and at the same time it is interpreted as a coupling or source for an operator in the dual field theory. When we do the path integration over the fields in AdS, we have to keep the boundary values $\Phi_0(x)$ fixed. What we obtained finally is a functional $Z[J]$ of the form:

$$Z[J] = \int_{J(x)=\Phi_0} [\mathrm{d}\Phi]\ \exp(-\mathrm{i}S[\Phi]), \tag{5}$$

where the source $J(x)$ is the boundary field $\Phi_0(x)$. This source $J(x)$ couples to a (gauge invariant) operator $O(x)$ with conformal dimension Δ_+ in the field theory[1)]. Performing functional differentiation of eq. (5) with respect to the sources, we can obtain the connected correlation functions of the gauge invariant operators $O(x)$ in the quantum field theory:

$$\langle O_1(x_1)\cdots O_n(x_n)\rangle = \frac{\delta^n \log Z}{\delta J_1(x_1)\cdots\delta J_n(x_n)}\,. \tag{6}$$

These are of course rather formal expressions. In general one does not know how to do this type of path integral including the metric degrees of freedom or even the proper string theory dual. In the large N_c and large coupling $g^2_{\mathrm{YM}}N_c$ limit, the gravitational theory becomes classical. The path integral eq. (5) now is dominated by the classical solutions from the equations of motion for fields. The generating functional $\log Z$ can be simplified and computed by the classical action evaluated on the classical solution. In this case in the asymptotic expansion eq. (4) the coefficient $\Phi_1(x)$ is the vacuum expectation value of the dual operator sourced by Φ_0:

$$\langle O(x)\rangle \propto \Phi_1(x). \tag{7}$$

This scheme applies to all fields in AdS, also to the metric itself. The operator that corresponds to the metric is the energy-momentum tensor. In the same way the operator that corresponds to a gauge field in AdS is a current. The essentials of the holographic dictionary are summarized in Table 1.

One can use this dictionary to generate new solutions that are deformations of the simple AdS space (eq. (1)) by switching on certain couplings. In practice this means that one demands specific boundary conditions on suitably chosen AdS fields that represent couplings in the dual field theory. Let us now explain how this strategy can be implemented to obtain a holographic version of a Weyl semimetal.

3 The holographic Weyl semimetal

To find the holographic background solution we first must identify what kind of deformations we need to introduce in AdS space to mimic the essential features of a Weyl semimetal. In order to do so we first review quickly a quantum field theoretical model of a Weyl semimetal.

3.1 Weyl semimetal from Dirac equation

In Weyl semimetal, the physics around the nodal points can be described by a quantum field theoretical model which takes the following form of a "Lorentz breaking" Dirac equation [26, 27]:

$$(\mathrm{i}\partial\!\!\!/ - eV\!\!\!/ - \gamma_5 \boldsymbol{\gamma}\cdot\mathbf{b} + M)\,\psi = 0\,, \tag{8}$$

where $X\!\!\!/ = \gamma^\mu X_\mu$ with $X_\mu \in \{\partial_\mu, V_\mu\}$, V_μ is the electromagnetic gauge potential, γ^μ is the Dirac matrices, and $\gamma_5 = \mathrm{i}\gamma_0\gamma_1\gamma_2\gamma_3$. We can define left- or right-handed spinors via $(1 \pm \gamma_5)\psi = \psi_{\mathrm{L,R}}$. The axial gauge field $\mathbf{b}$ breaks the time reversal

Table 1 The essentials of the holographic dictionary

Field in AdS	Dual operator
Metric $g_{\mu\nu}$	Energy-momentum tensor $T^{\mu\nu}$
Gauge field A_μ	Current J^μ
Scalar field Φ	Scalar operator O

1) This choice is known as standard quantization. When $\frac{d}{2} \leq \Delta_+ \leq \frac{d}{2} + 1$, for the dual field theory we could add a double trace deformation $\int \mathrm{d}^d x O(x)^2$ which is irrelevant close to the fixed point, to generate a flow to a new fixed point. In this case Δ_+ and Δ_- exchange their roles, i.e., $\Phi_1(x)$ is now interpreted as the source $J(x)$ which couples to an operator $O(x)$ of conformal dimension Δ_-. This is known as alternative quantization of the bulk theory [25].

symmetry and is introduced to separate the Weyl points in the momentum space as we will show from the perspectives of energy spectrum. For simplicity we take $\mathbf{b} = b\mathbf{e}_z$. M is the mass of the Dirac field.

The energy spectrum of eq. (8) is shown in Figure 1. When $|b| > |M|$ the spectrum is ungapped. There is a band inversion in the spectrum and at the crossing points the wave function is described by the one of Weyl fermions. The separation of the Weyl points in momentum space is given by $2\sqrt{b^2 - M^2}$ along the direction indicated by the vector $\mathbf{b}$. At low energies it is described by the the effective theory with the Lagrangian of the form eq. (8) with $M_{\rm eff} = 0$ and $\mathbf{b}_{\rm eff} = \sqrt{b^2 - M^2}\mathbf{e}_z$. For $|b| < |M|$ the system is gapped with gap $2M_{\rm eff} = 2(|M| - |b|)$.

The axial anomaly

$$\partial_\mu J_5^\mu = \frac{1}{16\pi^2}\varepsilon^{\mu\nu\rho\lambda}F_{\mu\nu}F_{\rho\lambda} + 2M\bar{\psi}\gamma_5\psi \tag{9}$$

indicates there is an anomalous Hall effect in the Weyl semimetal phase [28-33]

$$\mathbf{J} = \frac{1}{2\pi^2}\mathbf{b}_{\rm eff}\times\mathbf{E}\,. \tag{10}$$

Thus by tuning M/b, from the band structure we see that there is a quantum phase transition from topologically nontrivial Weyl semimetal phase to a trivial insulating phase. This phase transition is beyond the Landau classification and is an example of a topological phase transition. In both phases of the system, the same symmetries of the underlying theory are explicitly broken by the the couplings M, b. Due to the fact that in the topologically nontrivial phase there is a nontrivial Hall effect while in the topological trivial phase there is trivial Hall effect, the Hall conductivity can be taken as the order parameter[2)] of this special topological phase transition [34]. In more general case, additional massless Dirac fermions might show up, and the topologically trivial phase might be a semimetal instead of a gapped trivial phase. Then this quantum phase transition goes from a topologically nontrivial semimetal to a trivial semimetal. This will be exactly the case of our holographic model in the next subsection. In sect. 4 we will improve on this and discuss a holographic model with a phase transition to a Chern insulator.

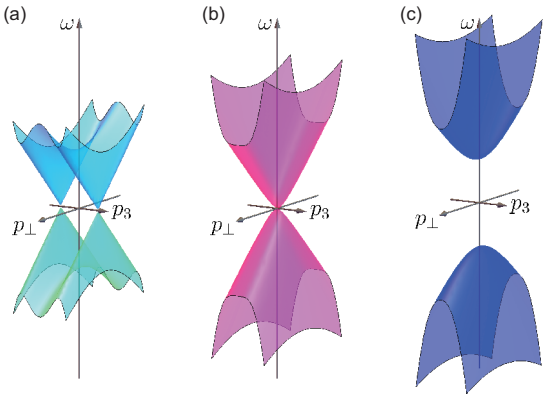

Figure 1 (Color online) Phases of the Dirac equation (eq. (8)). The figure shows the dispersion relation as a function of $p_\perp$ and p_3. (a) Deep in the Weyl semimetal phase; (b) the critical point in between the two; (c) the gapped phase.

The anomalous Hall effect (eq. (10)) in the quantum field theory is obtained from a one-loop contribution to the polarization tensor. However, there are infamous regularization ambiguities [35] in the quantum field theory. There are some ways to resolve the ambiguity, e.g. by considering anomaly cancellation arising from chiral edge states at the boundaries (Fermi arcs) [36] or by matching to a tight-binding model [26, 33].

What can we learn from this for building a holographic model? First we see that there are two $U(1)$ symmetries at play. One of them, the axial one, is anomalous and explicitly broken by the mass term in the Dirac equation. The anomaly gives rise to the quantum Hall effect eq. (10) as long as $\sqrt{b^2 - M^2} > 0$. The mass term can be identified as a source for the operator $\bar{\psi}\psi$. We can take the mass to be the expectation value of a complex classical scalar field that is charged under the axial $U(1)$ symmetry. Because of this an expectation value breaks the axial symmetry already on the classical level. Under a chiral rotation $\psi \to \mathrm{i}\alpha\gamma_5\psi$ the operator $\bar{\psi}\psi$ transforms into $\bar{\psi}\psi \to 2\mathrm{i}\alpha\bar{\psi}\gamma_5\psi$. Furthermore the parameter $\mathbf{b}$ or more generally b^μ couples to the axial current $J_5^\mu = \bar{\psi}\gamma_5\gamma^\mu\psi$ and can therefore be understood as the background value of an axial gauge field. These considerations give us the ingredients we need to implement in the holographic model.

3.2 Holographic model

A holographic action allowing the implementation of the above symmetries and breaking pattern is

$$\begin{aligned} S = \int \mathrm{d}^5x\sqrt{-g}\Big[&\frac{1}{2\kappa^2}\Big(R + \frac{12}{L^2}\Big) - \frac{1}{4}\mathcal{F}^2 - \frac{1}{4}F^2 \\ &+ \epsilon^{abcde}A_a\Big(\frac{\alpha}{3}\big(F_{bc}F_{de} + 3\mathcal{F}_{bc}\mathcal{F}_{de}\big) + \zeta R^f{}_{gbc}R^g{}_{fde}\Big) \\ &- (D_a\Phi)^*(D^a\Phi) - V(\Phi)\Big], \end{aligned} \tag{11}$$

where κ^2 is the Newton constant, L is the AdS radius and α, ζ are the Chern-Simons coupling constants[3)]. In field the-

2) It is not a traditional order parameter but Hall effect is known to serve as signature of topologically non-trivial Fermi surfaces [28].

3) Note that $\epsilon_{abcde} = \sqrt{-g}\varepsilon_{abcde}$ with $\varepsilon_{0123r} = 1$. Our conventions for indexes are as follows: latin indexes from the beginning of the alphabet $\{a, b, \dots\}$ are five dimensional ones, greek indexes are four dimensional ones and latin indexes from the middle of the alphabet $\{i, j, m, n\}$ are purely spatial indexes.

ory, we have conserved electromagnetic current and non-conserved axial current. As shown in Table 1, the conserved currents in the field theory are dual to gauge fields in AdS space. The electromagnetic $U(1)$ current is dual to the bulk gauge field $V_{\rm a}$ in AdS with field strength $\mathcal{F} = {\rm d}V$. The axial $U(1)$ current is dual to the gauge field $A_{\rm a}$ in AdS with field strength $F = {\rm d}A$. Since the axial symmetry is anomalous in the field theory and in the bulk the anomaly is characterized by the Chern-Simons part of the action (eq. (11)) with coupling constants α and ζ. The gauge invariant regularization corresponds to this choice of Chern-Simons term with which the electromagnetic $U(1)$ symmetry remains non-anomalous. The anomaly arises in a gauge variation of the axial gauge field $\delta A_{\rm a} = \partial_{\rm a}\theta$ as a boundary term:

$$\mathcal{A} = \int {\rm d}^4x\sqrt{-g}\theta\Big(\frac{\alpha}{3}\epsilon^{\mu\nu\rho\lambda}\Big(F_{\mu\nu}F_{\rho\lambda}+3\mathcal{F}_{\mu\nu}\mathcal{F}_{\rho\lambda}\Big)+\zeta R^{\alpha}{}_{\beta\mu\nu}R^{\beta}{}_{\alpha\rho\lambda}\Big)\,. \tag{12}$$

We have included here the usual axial anomaly due to electromagnetic field, the purely axial anomaly due to axial gauge fields and the gravitational[4] contribution to the axial anomaly. All three will play a role in the physics of holographic Weyl semimetals. The factor of 3 in the axial anomaly reflects the symmetry factor that arises in the corresponding triangle diagram in quantum field theory. We will introduce the mass deformation via a boundary value of the scalar field Φ [37]. Since the dual axial symmetry is explicitly broken, in the bulk this scalar field is introduced to be only axially charged. The covariant derivative is $D_{\rm a}\Phi = (\partial_{\rm a} - {\rm i}qA_{\rm a})\Phi$. The scalar field potential is $m^2|\Phi|^2+\frac{\lambda}{2}|\Phi|^4$. The AdS bulk mass $m^2L^2 = -3$ is chosen such that the dual operator has conformal dimension three and its source has conformal dimension one. The electromagnetic and axial currents[5] are defined as:

$$J^{\mu} = \lim_{r\to\infty}\sqrt{-g}\Big(\mathcal{F}^{\mu r}+4\alpha\epsilon^{r\mu\beta\rho\sigma}A_{\beta}\mathcal{F}_{\rho\sigma}\Big)\,, \tag{13}$$

$$J^{\mu}_5 = \lim_{r\to\infty}\sqrt{-g}\Big(F^{\mu r}+\frac{4\alpha}{3}\epsilon^{r\mu\beta\rho\sigma}A_{\beta}F_{\rho\sigma}\Big)\,. \tag{14}$$

The model was first studied in the probe limit in ref. [38] and then in the backreacted case in ref. [39].

We are looking for asymptotically AdS solutions. The mass parameter and the time-reversal symmetry breaking parameter in the field theory are introduced through the conformal boundary conditions:

$$\lim_{r\to\infty} r\Phi = M\,,\quad \lim_{r\to\infty} A_z = b\,. \tag{15}$$

We take the following ansatz for the zero temperature solution:

$$\begin{aligned} &{\rm d}s^2 = u(-{\rm d}t^2+{\rm d}x^2+{\rm d}y^2)+\frac{{\rm d}r^2}{u}+h{\rm d}z^2\,,\\ &A = A_z{\rm d}z\,,\quad \Phi = \phi\,, \end{aligned} \tag{16}$$

where u, h, A_z, ϕ are functions of r. In this case M/b is the only tunable parameter of the system due to the conformal symmetry. We set $2\kappa^2 = L = 1$.

Critical solution The following Lifshitz solution is an exact solution of the system:

$$\begin{aligned} &{\rm d}s^2 = u_0r^2(-{\rm d}t^2+{\rm d}x^2+{\rm d}y^2)+\frac{{\rm d}r^2}{u_0r^2}+h_0r^{2\beta}{\rm d}z^2\,,\\ &A_z = r^{\beta},\quad \phi = \phi_0\,. \end{aligned} \tag{17}$$

It exists an anisotropic Lifshitz symmetry $(t, x, y, r^{-1}) \to s(t, x, y, r^{-1})$ and $z \to s^{\beta}z$. The irrelevant deformations can be introduced to flow it to UV with the boundary conditions eq. (15). The four constants $\{u_0, h_0, \beta, \phi_0\}$ in eq. (17) are determined by the values of λ, m and q.

It turns out that the following irrelevant perturbations around the Lifshitz fix point can flow the geometry to asymptotic AdS $u = u_0r^2(1+\delta u\, r^{\alpha})$, $h = h_0r^{\beta}(1+\delta h\, r^{\alpha})$, $A_z = r^{\beta}(1+\delta a\, r^{\alpha})$, $\phi = \phi_0(1+\delta\phi\, r^{\alpha})$. Only the sign of $\delta\phi$ is a free parameter and the geometry can flow to AdS with $\delta\phi = -1$. In the case $q = 1, \lambda = 1/10$, we have $(u_0, h_0, \beta, \phi_0, \alpha) \simeq (1.468, 0.344, 0.407, 0.947, 1.315)$ and $(\delta u, \delta h, \delta a) \simeq (0.369, -2.797, 0.137)\delta\phi$. We obtain the critical value $M/b \simeq 0.744$, which corresponds to the transition point.

Topological nontrivial phase At leading order the second type of solution in the IR is

$$\begin{aligned} &u = r^2,\ \ h = r^2,\ \ A_z = a_1+\frac{\pi a_1^2\phi_1^2}{16r}{\rm e}^{-\frac{2a_1q}{r}}\,,\\ &\phi = \sqrt{\pi}\phi_1\Big(\frac{a_1q}{2r}\Big)^{3/2}{\rm e}^{-\frac{a_1q}{r}}\,, \end{aligned} \tag{18}$$

a_1 can be set to a numerically convenient value. Later on we rescale to $b = 1$.

Starting from the near horizon solution eq. (18), the equations can be numerically integrated towards the UV. ϕ_1 can be taken as the shooting parameter to obtain an AdS_5 to AdS_5 domain wall. For the values $q = 1, \lambda = 1/10$ this type of solution exists only for $M/b < 0.744$.

Topological trivial phase The third type of solution at leading order in IR is

$$u = \Big(1+\frac{3}{8\lambda}\Big)r^2,\ \ h = r^2,\ \ A_z = a_1r^{\beta_1},\ \ \phi = \sqrt{\frac{3}{\lambda}}+\phi_1r^{\beta_2}\,, \tag{19}$$

4) A contribution due to the extrisic curvature vanishes on asymptotic boundary of AdS [22].

5) These are the consistent currents. The vector current J^{μ} is conserved while the conservation of the the axial current J^{μ}_5 is broken explicitly by the scalar field and spontaneously by the anomaly [37]. The covariant currents can be defined by dropping the Chern-Simons terms.

where $(\beta_1,\beta_2) = \left(\sqrt{1+\frac{48q^2}{3+8\lambda}}-1, 2\sqrt{\frac{3+20\lambda}{3+8\lambda}}-2\right)$. For our choice of λ and q $(\beta_1,\beta_2) = \left(\sqrt{\frac{259}{19}}-1, \frac{10}{\sqrt{19}}-2\right)$. a_1 can be set to be 1. ϕ_1 can be taken as the shooting parameter to obtain the AdS_5 to AdS_5 domain wall. For the values $q = 1, \lambda = 1/10$ this type of solution only exist for $M/b > 0.744$.

Figure 2 shows the profiles of the scalar field ϕ and the gauge field A_z. Only one of the above three types of solutions exists at a given value of M/b. The horizon value of A_z varies continuously between the two phases while the horizon value of ϕ jumps discontinuously. Close to the phase transition point, the deep IR geometry eq. (18) or (19) quickly flows to the critical Lifshitz solution in the intermediate IR region.

The free energy density can be computed by adding standard holographic counterterms and is behaved continuously and smoothly at the critical value [39]. Note that the free energy does not depend on the Chern-Simons coupling constant. It does not probe the topological nature of the quantum phase transition, in contrast to the anomalous Hall conductivity.

3.3 Anomalous Hall conductivity

The essential hall-mark of the topological character of the Weyl semimetal state is the presence of anomalous Hall conductivity. In the case we are interested in it is anomalous Hall conductivity for the vector type current. A fast way of calculating it in holography is as follows. First one observes that the quantity

$$j^\mu(r) = \mathcal{F}^{\mu r} + 4\alpha\epsilon^{r\mu\beta\rho\sigma}A_\beta\mathcal{F}_{\rho\sigma} \tag{20}$$

fulfills a radial conservation equations as a consequence of the holographic equations of motion in the bulk space-time

$$\frac{\mathrm{d}}{\mathrm{d}r}j^\mu(r) = \partial^\mu X\,. \tag{21}$$

The precise form of X is not important since from now on we integrate over space and take the zero frequency limit such that the right hand side of this conservation equation vanishes. It follows then that in this situation the holographic expectation value of the current is given by the value of $j^\mu(r)$ at the horizon:

$$J^\mu = j^\mu(r_h)\,. \tag{22}$$

Since due to the Bianchi identity the electric field is constant along the AdS bulk direction r, the current at zero temperature is given by the Hall current [40]:

$$J^x = 8\alpha A_z(0)E_y\,. \tag{23}$$

The anomalous Hall conductivity is completely determined by the horizon value of the axial gauge field [38, 39]. In particular in holography it is only non-vanishing in the topological phase but vanishes at the quantum critical point and in the non-topological phase. This is exactly the same behavior the weak coupling Dirac like model shows. The anomalous Hall conductivity (eq. (23)) is shown in Figure 3 for different values of model parameters.

3.4 Universality of the quantum phase transition

The precise value of M/b at which the topological quantum phase transition from the Weyl semimetal to the trivial theory arises depends on the model parameters. Using the holographic duality one can investigate the critical values of M/b as a function of the quartic scalar self coupling λ for various values of the axial charge q of the scalar field [40]. The result is shown in Figure 4.

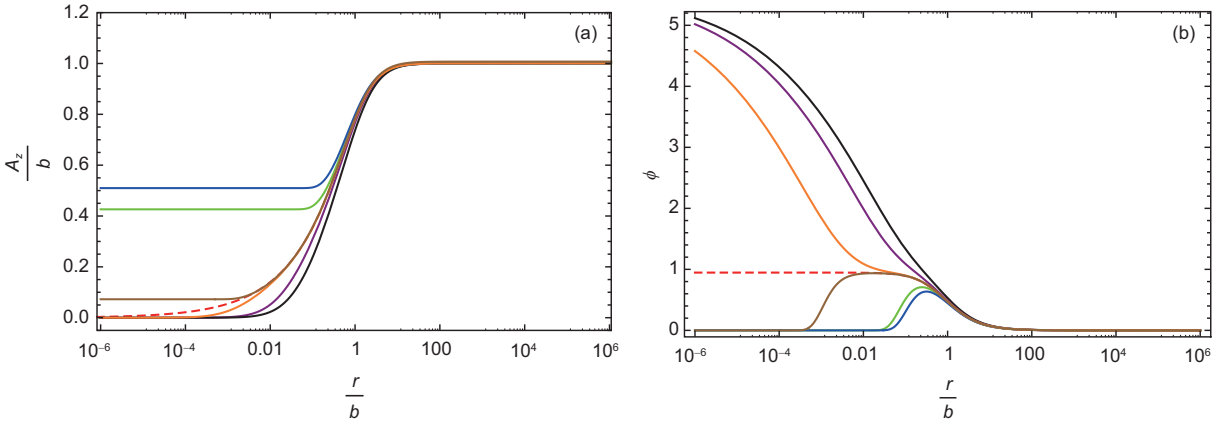

Figure 2 (Color online) The bulk profile of background A_z (a) and ϕ (b) for $M/b = 0.695$ (blue), 0.719 (green), 0.743 (brown), 0.744 (red-dashed), 0.745 (orange), 0.778 (purple), 0.856 (black). Figures from ref. [39].

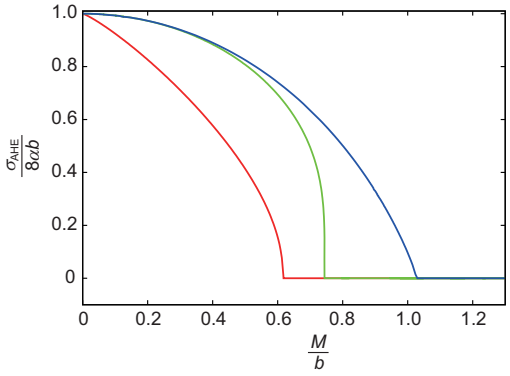

Figure 3 (Color online) The zero temperature anomalous Hall conductivity is given by the value of the axial gauge field on the degeneratre horizon at $r = 0$. It is plotted here for different model parameters, specifically $m^2 = -2$, $\lambda = 1/10$ (red), $m^2 = -3$, $\lambda = 1/10$ (green), $m^2 = -3$, $\lambda = 1$ (blue). It can be observed how the critical value for the M/b parameter where the conductivity goes to zero changes in the different cases. Figure from ref. [40].

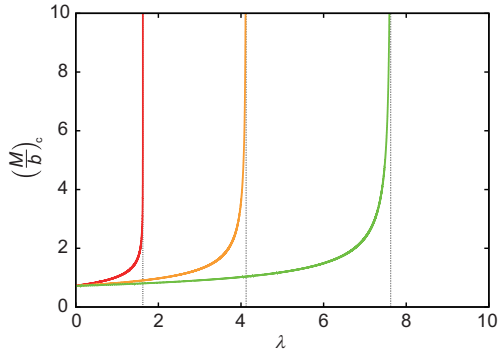

Figure 4 (Color online) The critical value of M/b as a function of the quartic scalar self coupling λ for different values of the axial charge $q = 1$, $q = 1.5$ and $q = 2$. As can be seen the value of M/b diverges at some finite values of λ. This means that in these cases the scalar self interaction suppresses the phase transition to the trivial phase. Figure from ref. [40].

Interestingly for a given charge value there is a maximum value of λ beyond which the phase transition does not occur at any finite value of M/b. This has an interesting interpretation in terms of the holographic duality. The spacetime curvature can be taken as a measure of the degrees of freedom. In the cases in which the phase transition cannot take place anymore it turns out that the holographic number of degrees of freedom in the infrared in the trivial phase would be larger than in the critical phase. Intuitively one expects that more degrees of freedom are gapped out in the IR than at the critical point. This intuition would be violated if the trivial phase could still be reached for high values of the self coupling. Fortunately direct inspection shows that this is not the case.

3.5 Holographic Fermi arcs

One of the key signatures of Weyl semimetals is the presence of topologically protected surface states, the so-called Fermi-arcs. A simple and efficient field theory model of Fermi arcs follows from the thinking about the low energy description in terms of the deformed Dirac operator (eq. (8)). The effective separation of the Weyl cones in the Brillouin zone enters the Dirac equation like a gauge field with the key difference that it couples with different signs to left- and right-handed Weyl fermions. If this parameter varies spatially it can induce an axial magnetic field $\mathbf{b}_5 = \nabla \times \mathbf{b}$. A standard argument shows now that such a spatial dependence is inevitable. Inside the Weyl semimetal we describe the system by a Dirac equation with axial gauge field $\mathbf{A}_5 = \mathbf{b}$. But outside the material there are no low energy states available for the electrons. This is equivalent to describing the outside by a Dirac equation with a very large mass and vanishing axial gauge field. In turn this means that on the edge of the material there is necessarily a strongly localized axial magnetic field. Now one can invoke an index theorem that states that the number of zero modes in the axial magnetic field is given by the degeneracy of the Lowest Landau level $|\mathbf{b}_5|/(2\pi)$. In a usual magnetic field there would be zero-modes of both chiralities but in the axial magnetic field the zero modes from both the right-handed and left-handed fermions have the same chirality. If one populates these zero modes by turning on a chemical potential they will lead to an edge current of the form:

$$\mathbf{J}_{\text{edge}} = \frac{\mu}{2\pi^2}\mathbf{b}_5 \,. \tag{24}$$

This can also be viewed as an instance of an anomaly induced transport phenomenon, the axial magnetic effect [17].

At strong coupling or more generally in the absence of quasiparticle excitations Fermi-arcs per se can not be expected to be seen. But the topologically protected edge currents should still exist[6]. This is exactly what ref. [41] investigated. The authors numerically constructed solutions with spatial dependent boundary conditions of the form:

$$A_z(r,x)\Big|_{r\to\infty} = \begin{cases} b_{\text{L}}, & \text{for} \quad x < -l, \\ p(x), & \text{for} \quad -l \geq x \leq l, \\ b_{\text{R}}, & \text{for} \quad x > l, \end{cases} \tag{25}$$

where $p(x)$ is a suitably chosen smooth interpolating function. The scalar field was kept fixed and the chemical potential is introduced as:

$$\lim_{r\to\infty} r\Phi(r) = M, \quad \lim_{r\to\infty} V_t = \mu \,, \tag{26}$$

6) It might be however that Fermi arcs exist also in the spectral functions of probe fermions. Indeed as we will review in the next section, probe fermions do carry the signatures of the non-trivial topology of momentum space.

with the understanding that $V_t = 0$ at the horizon. They found that indeed a current flows on the interface between the two asumptotic regions and the total current in the y direction is given by

$$J_y = 8\alpha\mu(b_{\text{eff,L}} - b_{\text{eff,L}}) = 8\alpha\mu\left(\sigma_{\text{AHE,L}} - \sigma_{\text{AHE,R}}\right) . \tag{27}$$

This is exactly what one can expect since in the effective low energy theory $\int \mathrm{d}x B_5 = b_{\text{eff,L}} - b_{\text{eff,R}}$. Moreover, the current distribution is concentrated on the interface as can be seen from Figure 5.

3.6 Fermionic probes and the topological invariant

Various bulk calculations have shown that the dual system should be a Weyl semimetal having Weyl cones with an effective momentum separation in the direction of **b**. A direct observation of the Weyl cones needs to employ the holographic fermionic probes whose spectral function at zero temperature would show two poles separated in the momentum space in the **b** direction. Besides a direct observation of the two Weyl cones, an important further evidence is to compute the topological invariant for the dual strongly coupled topological semimetal states, which would also require a calculation of the Green's function of probe fermions in the bulk. In the following we will first introduce how topological invariants for strongly coupled systems could be calculated directly from the bulk fermionic Green's function and then show how fermionic spectral functions could be calculated for the holographic Weyl semimetal background and obtain the corresponding topological invariant accordingly.

Mathematically topological invariants are properties that are invariant under homeomorphisms. Similarly in physics

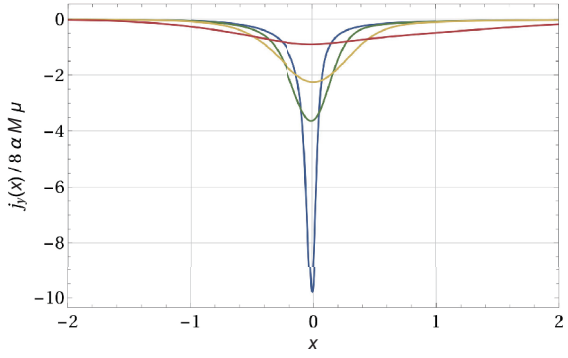

Figure 5 (Color online) Current distribution along the x-direction for different choices of interpolating functions with widths $l = 0.1, 0.5, 1, 4$. As expected the current in localized in the region in which the effective low energy axial gauge field shows non-vanishing curl. This is the direct holographic counterpart of the Fermi-arcs associated to the surface of a Weyl semimetals. Figure with permission reproduced from ref. [41], ©2017 by the American Physical Society.

topological invariants can be defined for topological matter, which are invariant under adiabatic deformations of the Hamiltonian that protect the topology of the underlying system.

For weakly coupled topological systems, in momentum space we can define the topological invariants from the Bloch states, i.e. the eigenstates of the weakly coupled Hamiltonians. The Berry phase [42], which is the phase accumulated along a closed loop γ in the momentum space for the Bloch states $|n_{\mathbf{k}}\rangle$, is defined as $\phi = \oint_\gamma \mathcal{A}_{\mathbf{k}} \cdot \mathrm{d}\mathbf{k}$ where the Berry connection is determined by the eigenstates $|n_{\mathbf{k}}\rangle$ of the momentum space Hamiltonian as $\mathcal{A}_{\mathbf{k}} = \mathrm{i}\sum_j \langle n_{\mathbf{k}}|\partial_{\mathbf{k}}|n_{\mathbf{k}}\rangle$ with j runs over all occupied bands. The Berry phase with value 0 or π is one simple example of a topological invariant.

There is another way to compute the Berry phase. Using the Berry curvature $\Omega_i = \epsilon_{ijl}(\partial_{k_j}\mathcal{A}_{k_l} - \partial_{k_l}\mathcal{A}_{k_j})$ associated to the the Berry connection and choosing a surface S whose boundary is the closed loop γ, we have $\phi = \int_S \mathbf{\Omega} \cdot \mathrm{d}\mathbf{S}$.

An equivalent way to calculate the topological invariant is to use the Green's function:

$$N(k_z) = \frac{1}{24\pi^2}\int \mathrm{d}k_0 \mathrm{d}k_x \mathrm{d}k_y \mathrm{Tr}\left[\epsilon^{\mu\nu\rho z} G\partial_\mu G^{-1} G\partial_\nu G^{-1} G\partial_\rho G^{-1}\right], \tag{28}$$

where $\mu, \nu, \rho \in k_0, k_x, k_y$ and $k_0 = \mathrm{i}\omega$ is the Matsubara frequency. For free systems, the Green's function takes the form $G(\mathrm{i}\omega, k) = 1/(\mathrm{i}\omega - h(k))$ where $h(k)$ is the Hamiltonian matrix $H = \sum_k c_k^\dagger h(k) c_k$. We can also use this formula to compute topological invariant for interacting systems, however, for strongly interacting systems it is difficult to compute practically since it involves an integration in the $\mathrm{i}\omega$ direction.

Refs. [43-45] show that the Green's function at zero frequency $G(0, \mathbf{k})$ contains all the topological information of the system. An effective topological Hamiltonian can be defined

$$\mathcal{H}_{\text{t}}(\mathbf{k}) = -G^{-1}(0, \mathbf{k}) \tag{29}$$

and the eigenvectors can be obtained from this effective topological Hamiltonian. As long as there is no pole at nonzero ω in $G(\mathrm{i}\omega, \mathbf{k})$, the topological invariants derived from the effective Hamiltonian $\mathcal{H}_{\text{t}}(\mathbf{k})$ would be the same as those defined in the original system. Thus topological invariants can be defined using negative valued eigenvectors of $\mathcal{H}_{\text{t}}(\mathbf{k})$, i.e. effective occupied states $n_{\mathbf{k}}$ with $\mathcal{H}_{\text{t}}(\mathbf{k})|n_{\mathbf{k}}\rangle = -E_{\text{t}}|n_{\mathbf{k}}\rangle$ and $E_{\text{t}} > 0$.

Having shown that topological invariants for strongly coupled fermionic systems could be directly calculated from the zero frequency Green's function, we now show how fermionic Green's function could be calculated for the holographic Weyl semimetal. In holography, probe fermions in the bulk have been studied for various backgrounds at finite density in refs. [46, 47] to obtain the dual fermion spectral functions. Here for the holographic Weyl semimetal, to

probe the dual fermion spectrum we add a probe fermion on the background geometry (eq. (16)) and calculate the dual Green's functions from the holographic dictionary [48]. One important difference here is that we work in five dimensions, and now a bulk four component spinor corresponds to a two component spinor of the dual field theory in four dimensions [49]. Therefore in the bulk we use two spinors Ψ_1 and Ψ_2 with opposite sign masses and axial charges and choose one with standard quantization while the other with alternative quantization to correspond to four component spinor with two opposite chiralities.

From the point of view of the dual field theory these probe fermions correspond to composite operators of a scalar field with the fundamental fermions. A priori it is these fundamental fermions that carry the non-trivial topology. As we will show now this topology is still present in the strongly coupled bound state that are the probe fermions.

The action of probe fermions is as follows:

$$\begin{aligned} S &= S_1 + S_2 + S_{\rm int}\,, \\ S_1 &= \int \mathrm{d}^5x\,\sqrt{-g}\mathrm{i}\bar{\Psi}_1(\Gamma^a D_a - m_f - \mathrm{i}A_a\Gamma^a)\Psi_1\,, \\ S_2 &= \int \mathrm{d}^5x\,\sqrt{-g}\mathrm{i}\bar{\Psi}_2(\Gamma^a D_a + m_f + \mathrm{i}A_a\Gamma^a)\Psi_2\,, \\ S_{\rm int} &= -\int \mathrm{d}^5x\,\sqrt{-g}(\mathrm{i}\eta_1\Phi\bar{\Psi}_1\Psi_2 + \mathrm{i}\eta_1^*\Phi^*\bar{\Psi}_2\Psi_1)\,, \end{aligned} \tag{30}$$

where $D_a = \partial_a - \frac{\mathrm{i}}{4}\omega_{\underline{mn},a}\Gamma^{\underline{mn}}$. The coupling constant in front of A_z is opposite for the two spinors. Here $\Gamma^a = e^a_{\ \underline{m}}\Gamma^{\underline{m}}$ with $\Gamma^{\underline{m}}$ the Γ-matrices in five dimensional Minkowski spacetime.

From this form of bulk action for probe fermions, we can obtain the retarded Green's function from the boundary values of the two bulk fermionic fields at different momenta [48]. In the simplest $M/b \to 0$ limit, it could easily been shown that two poles exist separately in the z direction in the momentum space. At small M/b limit, this could also be obtained with some semi-analytic method.

As a simple example we first show how this procedure works for the pure AdS case, which of course would give a trivial topological invariant. In this case, in fact the system is degenerate at zero frequency, i.e. the two Weyl nodes coincide to form a Dirac node. The fermionic retarded Green's functions for one chirality for $\omega > k$ has already been obtained in ref. [49]. The topological Hamiltonian $\mathcal{H}_t$ is defined as $-G^{-1}(0,\mathbf{k})$ from eq. (29). The two eigenvectors are $|n_1\rangle = n_1^0(k_z + k, k_x + \mathrm{i}k_y, 0, 0)^{\mathrm{T}}$ and $|n_2\rangle = n_2^0(0, 0, k_z - k, k_x + \mathrm{i}k_y)^{\mathrm{T}}$ where $n_l^0 = 1/\sqrt{2k(k-(-1)^l k_z)}$ with $l \in \{1, 2\}$. In fact these two eigenvectors are the same as the ones in the free massless Dirac Hamiltonian. $|n_1\rangle$ has positive chirality and is the eigenvector of the positive chirality Hamiltonian while $|n_2\rangle$ has negative chirality and is the eigenvector of the negative chirality Hamiltonian.

The topological invariants can be calculated as follows. Around the Dirac node, we can define a sphere $\mathbf{S}$ to enclose it. On this sphere the system is gapped. The topological invariant can be computed from $C_l = \frac{1}{2\pi}\oint_S \mathbf{\Omega}_l \cdot \mathrm{d}\mathbf{S}$, where $\Omega^i = \epsilon^{ijk}\mathcal{F}_{ij}$ with $(i, j, k) \in \{k_x, k_y, k_z\}$ and $\mathcal{F}$ is the Berry curvature. Note that the topological number is an integer number and it stays as a constant when we deform the shape and exact shape and radius of the sphere without passing through a Dirac node. We can parameterize the sphere as $\mathbf{S} = k_0(\sin\theta\cos\phi, \sin\theta\sin\phi, \cos\theta)$ and we have $\mathbf{\Omega}_l = (-1)^l\mathbf{e}_\rho/2k_0^2$. We obtain $C_1 = -1$ for $|n_1\rangle$ and $C_2 = 1$ for $|n_2\rangle$. Then the total topological invariant is zero. This is due to the fact that the zero density state dual to pure AdS_5 is a Dirac semimetal.

Now we continue to calculate the topological invariants for the holographic Weyl semimetal. In Weyl semimetals, we can define the topological invariant as the integration of Berry curvature on a closed surface $\mathbf{S}$ which encloses one of the Weyl nodes in the momentum space. This result will be insensitive to the shape and size of the closed surface. From semi-analytic calculations, we obtained that when M/b is very small, the topological invariants are ± 1 which are precisely the same as the results from weakly coupled WSM model. For larger M/b numerics has to be involved. The topological invariant for finite temperature case has been studied in ref. [50]. The total topological invariants are zero due to the Nielsen-Ninomiya theorem [51].

In addition to the anomalous Hall conductivity and edge states, the nontrivial topological invariants serve as further nontrivial evidence that the holographic Weyl semimetal models are strongly coupled topologically nontrivial semimetals.

3.7 Finite temperature, conductivities and viscosities

In the previous subsections, the studies are mainly for the zero temperature case. Now we will turn to finite temperature physics and the interesting transport physics.

We use the following ansatz to study the finite temperature solutions [39]:

$$\begin{aligned} \mathrm{d}s^2 &= -u\mathrm{d}t^2 + \frac{\mathrm{d}r^2}{u} + f(\mathrm{d}x^2 + \mathrm{d}y^2) + h\mathrm{d}z^2\,, \\ A &= A_z\mathrm{d}z\,, \quad \Phi = \phi\,, \end{aligned} \tag{31}$$

where all the fields u, f, h, A_z, ϕ are functions of r. At the regular horizon $r = r_0$, u has a simple zero whereas all these functions are analytic. This geometry is a black hole with horizon located at $r = r_0$ and Hawking temperature $4\pi T = u'(r_0)$. According to the holographic dictionary, the Hawking temperature of this black hole geometry corresponds to the physical temperature of the dual field theory.

By using the scaling symmetries of the system and the constraints from the equations of motion near the horizon, there are only two independent dimensionless parameters, which can be parametrized by M/b and T/b in the UV.

A cartoon illustration for the phases is shown in Figure 6 [52]. At zero temperature the model undergoes the already discussed topological quantum phase transition between a topological semimetal state and a trivial semimetal state. At the critical phase transition point there is an emergent Lifshitz symmetry at zero temperature. At finite temperature there is a quantum critical regime whose physics is governed by the Lifshitz symmetry. Meanwhile, this quantum phase transition becomes a smooth crossover behavior.

Conductivities can be computed with Kubo formula via retarded correlation functions:

$$\sigma_{mn} = \lim_{\omega\to 0} \frac{1}{\mathrm{i}\omega} \langle J_m J_n \rangle(\omega, \mathbf{k} = 0) \,. \tag{32}$$

According to the holographic dictionary, we can obtain the retarded Green's functions by studying the gauge field fluctuations around the background with infalling boundary conditions at the horizon. We obtain

$$\sigma_{\mathrm{AHE}} = 8\alpha A_z(r_0) \,, \quad \sigma_{xx} = \sigma_{yy} = \sqrt{h(r_0)} \,. \tag{33}$$

From the fact that $r_0 = 0$ and $h(0) = 0$ at zero temperature one concludes that the diagonal conductivities vanish. The anomalous Hall effect (Figure 7) is completely determined by the horizon value of the axial gauge field.

The longitudinal electric conductivity can be computed by studying the fluctuation $\delta V_z = v_z \mathrm{e}^{-\mathrm{i}\omega t}$ in the bulk. At zero temperature we obtain $\sigma_{zz} = 0$ and for finite temperature $\sigma_{zz} = \left.\frac{f}{\sqrt{h}}\right|_{r=r_0}$.

The diagonal components of electric conductivities at finite temperature as a function of M/b is shown in Figure 8. We can see that at the critical value there is a peak (minimum) for the transverse (longitudianl) diagonal conductivities. Both the height of the peak and depth of the minimum grow with temperature. At zero M we have $\sigma_{xx,yy,zz} = \pi T$ and for large M the conductivities $\sigma_{xx,yy,zz} = c\pi T$ with a temperature independent c smaller than 1. This is due to that in the trivial phase some but not all degrees of freedom are gapped out. The quantum phase transition is between a topological semimetal and a trivial semimetal.

Now let us explain the behavior of viscosities in this system. It is known that in an axisymmetric system which has time reversal symmetry breaking by vector $\mathbf{b}$ there are seven[7] independent viscosities [53] in which two of them are independent odd viscosity tensor components. The viscosities can be computed from the Kubo formula

$$\eta_{ij,kl} = \lim_{\omega\to 0} \frac{1}{\omega} \mathrm{Im}[G^R_{ij,kl}(\omega, 0)] \,, \tag{34}$$

where the retarded Green's function of the energy momentum tensor

$$G^R_{ij,kl}(\omega, 0) = -\int \mathrm{d}t\mathrm{d}^3x \mathrm{e}^{\mathrm{i}\omega t}\theta(t)\langle[T_{ij}(t, \mathbf{x}), T_{kl}(0, 0)]\rangle \,. \tag{35}$$

Since we chose $\mathbf{b} = b\hat{e}_z$, the two shear viscosities [54-56] are obtained from the symmetric part of the retarded Green's function under the exchange of $(ij) \leftrightarrow (kl)$

$$\eta_\parallel = \eta_{xz,xz} = \eta_{yz,yz} \,, \qquad \eta_\perp = \eta_{xy,xy} = \eta_{T,T} \tag{36}$$

and the two odd or Hall components of viscosity are related to the antisymmetric part by

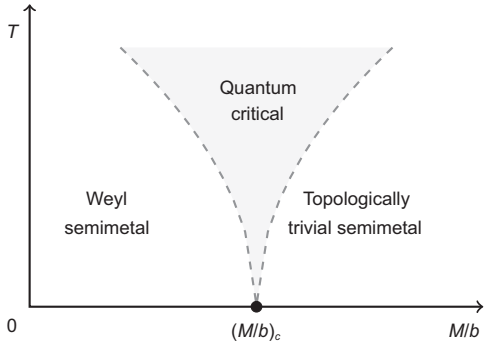

Figure 6 (Color online) The cartoon picture for the holographic Weyl semimetal at different temperatures as a function of M/b. Figure from ref. [39].

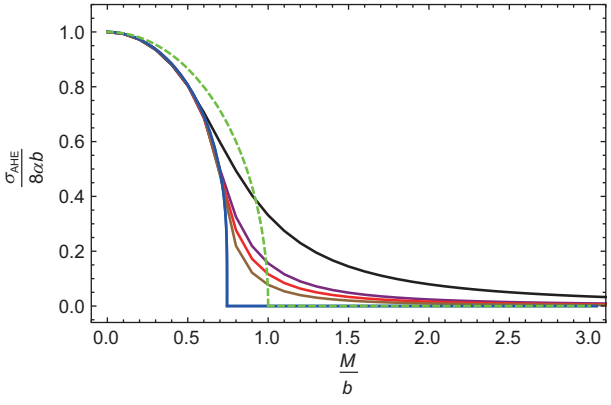

Figure 7 (Color online) Anomalous Hall conductivity as a function of M/b at different temperatures. The solid lines are obtained from the holographic Weyl semimetal. For zero temperature a sharp but continuous phase transition occurs at a critical value of M/b (blue), which becomes a smooth crossover at finite temperature. The curves are for $T/b = 0.1$ (black), 0.05 (purple), 0.04 (red), 0.03 (brown). The dashed (green) line is for the weak coupling model. Figure from ref. [39].

7) These seven components includ three shear viscosities, two odd viscosities and two bulk viscosities. We focus on four of them and will not consider the other two bulk viscosities and one shear viscosity which are from the spin zero sector.

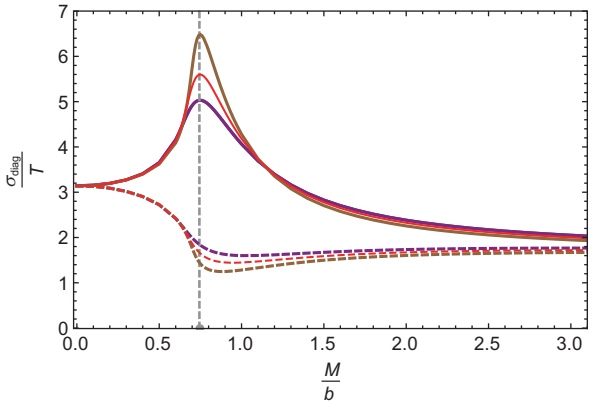

Figure 8 (Color online) The diagonal components of electric conductivities as a functional of M/b for different temperatures. The solid lines are for $\sigma_{xx} = \sigma_{yy}$ and the dashed lines are for σ_{zz} from holographic Weyl semimetal with $T/b = 0.05$ (purple), 0.04 (red), 0.03 (brown). The dashed gray line is the critical value of M/b at the topological quantum phase transition. Figure from ref. [39].

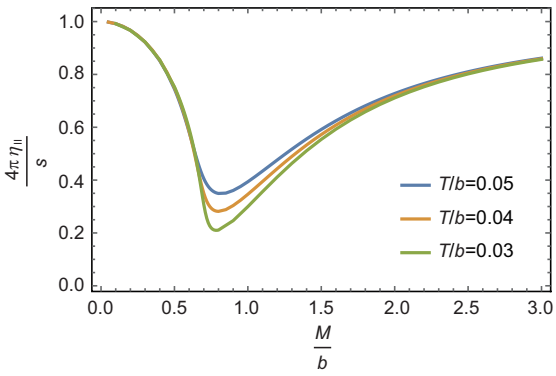

Figure 9 (Color online) The longitudinal shear viscosity over entropy density $4\pi\eta_{\parallel}/s$ as a function of M/b at different temperatures. Figure from ref. [52].

$$\eta_{H_\parallel} = -\eta_{xz,yz} = \eta_{yz,xz}\,, \quad \eta_{H_\perp} = \eta_{xy,T} = -\eta_{T,xy}, \tag{37}$$

where the index T denotes the component $xx - yy$. Note that $\eta_{H_\perp}$ is the odd or Hall viscosity in the plane orthogonal to **b** while $\eta_{H_\parallel}$ is specific to axisymmetric three dimensional systems[8)].

In holography the viscosities can be computed via switching on the following perturbations $\delta g_{iz} = h_{iz}(r)\mathrm{e}^{-\mathrm{i}\omega t}$, $\delta A_i = a_i(r)\mathrm{e}^{-\mathrm{i}\omega t}$ for $i \in \{x, y\}$. For the other components of viscosities can be computed by considering the perturbations $\delta g_{xx} - \delta g_{yy} = 2h_T(r)\mathrm{e}^{-\mathrm{i}\omega t}$, $\delta g_{xy} = h_{xy}(r)\,\mathrm{e}^{-\mathrm{i}\omega t}$. From the holographic dictionary we obtain the following viscosity coefficients:
dissipative viscosity:

$$\eta_\parallel = \eta_{xz,xz} = \eta_{yz,yz} = \left.\frac{f^2}{\sqrt{h}}\right|_{r=r_0}, \tag{38}$$

$$\eta_\perp = \eta_{xy,xy} = \eta_{T,T} = \left. f\sqrt{h}\right|_{r=r_0}, \tag{39}$$

dissipationless odd viscosity:

$$\eta_{H_\parallel} = \eta_{yz,xz} = -\eta_{xz,yz} = 4\zeta\left.\frac{q^2 A_z \phi^2 f^2}{h}\right|_{r=r_0}, \tag{40}$$

$$\eta_{H_\perp} = \eta_{xy,T} = -\eta_{T,xy} = 8\zeta q^2\phi^2 f A_z\Big|_{r=r_0}. \tag{41}$$

The dissipative viscosity is a form of shear viscosity and it is interesting to express it normalized to the entropy density $\frac{\eta_\parallel}{s} = \frac{f}{4\pi h}|_{r=r_0}$. As can be seen from Figure 9 the shear viscosity drops significantly below the standard result of KSS bound [58]. In view of the various results of violation of the KSS bound in anisotropic theories [59, 60] this is not unexpected. Still it is very interesting to note that the shear viscosity reaches a minimum in the quantum critical region of $M/b \approx 0.744$. In contrast the transverse viscosity obeys the KSS bound is exactly $\eta_\perp/s = 1/4\pi$.

A particular interesting fact about odd viscosities is that they are directly proportional to the mixed axial-gravitational anomalous constant which is the gravitational contribution to the axial anomaly ζ in eq. (12). Therefore at least in this holographic model they are a new example of an anomaly induced transport coefficient. Figure 10 shows the odd viscosities $\eta_{H_\parallel}$ and $\eta_{H_\perp}$ as a function of M/b at small but finite temperatures. In the topologically nontrivial phase the odd viscosity is highly suppressed. It rises steeply when M/b enters into the quantum critical region, peaks around the critical value of M/b and then falls off slowly when M/b increases. In the limit $M/b \to \infty$ the odd viscosity vanishes.

The appearance of odd viscosity in the quantum critical region can be considered to be a prediction from holography. Its relation to the gravitational anomaly suggests that this is a universal property. Indeed recently anomalous Hall viscosity has also been obtained in a weakly coupled quantum field theory model of the quantum critical point in ref. [61]. The relation to anomalies in the weakly coupled theory is far from clear. We expect that further investigation of the holographic model and its RG flow to the critical point can give valuable insight into the origin of this type of odd viscosity.

Note that from the analytic results on the viscosities and conductivities we obtain the non-trivial relation:

$$\frac{\eta_\parallel}{\eta_\perp} = \frac{2\eta_{H_\parallel}}{\eta_{H_\perp}} = \frac{\sigma_\parallel}{\sigma_\perp} = \left.\frac{f}{h}\right|_{r=r_0}, \tag{42}$$

8) There exists odd viscosity $\eta_{H_\parallel}$ by considering the coupling of elastic gauge fields to the electron gas in Weyl semimetals [57]. It was shown in ref. [57] that this effective odd viscosity is related to the Hall conductivity of the electron gas and arises from the electronic point of view as an axial Hall conductivity. Here in holography the Hall viscosity should be viewed as an intrinsic property of the strongly coupled electron fluid.

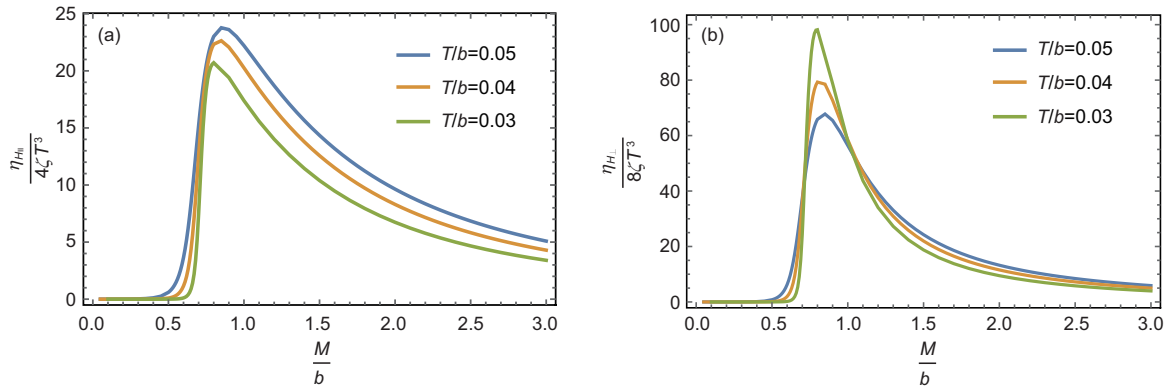

Figure 10 (Color online) Odd viscosity $\eta_{H_\parallel}$ (a) and $\eta_{H_\perp}$ (b) as a function of M/b at different temperatures. Figures from ref. [52].

where $\sigma_\parallel = \sigma_{zz} = \frac{f}{\sqrt{h}}\big|_{r=r_0}, \sigma_\perp = \sigma_{xx} = \sigma_{yy} = \sqrt{h}\big|_{r=r_0}$.

Furthermore, in the quantum critical regime there exists interesting temperature scaling behaviour of conductivities and viscosities. At $T = 0$, there is an emergent Lifshitz symmetry in the IR at the quantum phase transition point. The IR physics is invariant under $(t, x, y, r^{-1}) \to l(t, x, y, r^{-1}), z \to l^\beta z$ and $f \to l^{-2} f, h \to l^{-2\beta} h, A_z \to l^{-\beta} A_z, \phi \to \phi$, where β is the anisotropic scaling exponent [39]. At very low temperature, since $T \to l^{-1} T$ the temperature scaling dependence of the viscosities and conductivities near the critical region can be obtained from the scaling arguments. At the critical regime, we have $\eta_\parallel/s \propto T^{\gamma_1}, \eta_{H_\parallel} \propto T^{\gamma_2}, \eta_{H_\perp} \propto T^{\gamma_3}$ with $(\gamma_1, \gamma_2, \gamma_3) = (2 - 2\beta, 4 - \beta, 2 + \beta)$ and $\sigma_\parallel \propto T^{\gamma_4}, \sigma_\perp \propto T^{\gamma_5}, \sigma_{\mathrm{AHE}} \propto T^{\gamma_6}$ with $(\gamma_4, \gamma_5, \gamma_6) = (2 - \beta, \beta, \beta)$ for low temperatures. Figure 11 shows the temperature scaling exponents γ_i with $i \in \{1, \ldots, 6\}$ of the numerical results at low temperatures at the critical value of M/b. At sufficient low temperature, these scaling exponents approaches the analytic values from scaling analysics. Furthermore, the scaling behaviors explain the peak/dip behaviors of the conductivities/viscosities of holographic Weyl semimetal in the quantum critical regime.

The chiral vortical conductivity for the holographic Weyl semimetal has been calculated in ref. [62]. We can first compute the chiral vortical conductivity and then perform a suitable renormalization via the anomalous Hall conductivity and temperature squared. It was shown that at sufficiently low temperature this renormalized ratio stays as universal constants in both the Weyl semimetal phase and the quantum critical region. Furthermore, in the critical region the renormalized ratio is fully determined by the emergent Lifshitz scaling exponent at the critical point [62].

3.8 Axial Hall conductivity

Formally in quantum field theory the axial current can be coupled to an axial gauge field just as the electric current couples to the electric gauge field. There is however a big difference in the possible dynamics of these fields. The dynamics of the true gauge field is given by Maxwell's equations. For a gauge field that couples to an anomalous current, such as the axial current this is mathematically inconsistent. A simple way of seeing this is to note that Maxwells equations imply that the divergence of the current vanishes

$$\partial_\mu J^\mu = \partial_\mu \partial_\nu F^{\mu\nu} = 0\,. \tag{43}$$

In nature on a fundamental level anomalous currents are not coupled to gauge fields.

Nevertheless such fields can arise as effective fields in condensed matter systems. It has been shown in refs. [57,63-65] that axial electric and magnetic fields can be induced by applying strain on Weyl semimetals. These are effective low energy couplings in the theory and certainly do not obey Maxwell's equations and consequently do not jeopardize the consistency of the theory. Therefore it seems a legitimate physics question to ask if there is a purely axial analogue of the anomalous Hall effect in Weyl semimetals. This again is a question that can be nicely addressed in holographic models and leads to some important insights.

Since the anomalous Hall effect is a direct consequence of the anomaly let us have another look into it and see what could be expected. A remarkable fact is that the anomaly (eq. (12)) in the axial gauge fields is weaker by a factor of $1/3$ compared to the electromagnetic contribution. One useful way to think about this factor is to consider the origin of the anomaly in a triangle Feynman diagram. In the case of the purely axial anomaly this is a diagram with three identical axial currents on the vertices. Elementary Feynman rules instruct us therefore to multiply the diagram with a symmetry factor of $1/3!$. In comparison the electromagnetic contribution comes from a triangle diagram with two electric currents and one axial current. There are only two identical operators on the vertices and thus the symmetry factor is only $1/2!$ with gives a relative factor of $1/3$.

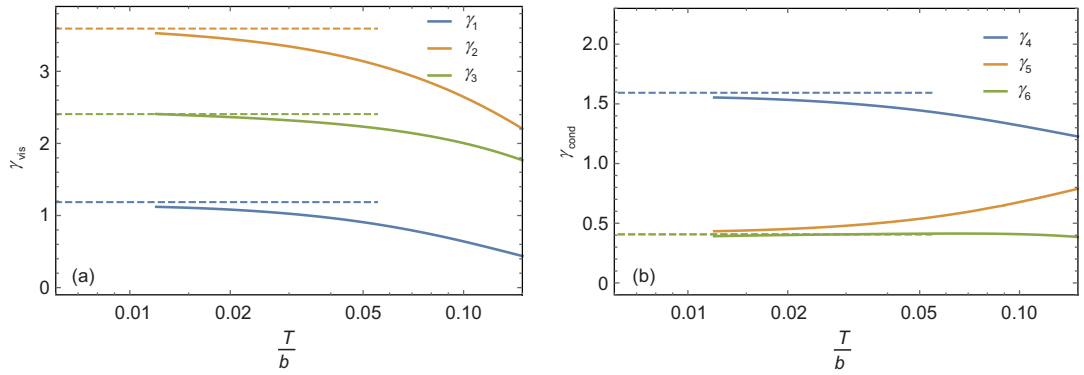

Figure 11 (Color online) The temperature scaling exponents γ_i with $i \in \{1, \ldots, 6\}$ for viscosities $\eta_{\|}$, $\eta_{H_{\|}}$ and $\eta_{H_\perp}$ (a) and for conductivities $\sigma_{\|}$, $\sigma_\perp$ and σ_{AHE} (b) in the quantum critical regime. The dashed lines represent the analytic values of the scaling exponents from the scaling analysis. Figures from ref. [52].

The natural expectation is therefore, that the purely axial Hall conductivity, e.g. the transverse axial current induced by an axial electric current is weaker by a factor of $1/3$ compared to the electric Hall conductivity.

While the electric Hall conductivity can be computed in an easy way from the horizon data, the calculation of the axial Hall conductivity is more cumbersome. It is complicated by the fact that the axial symmetry is broken not only by the anomaly but also by the expectation value of the scalar field (the dual of the mass term in the Dirac equation).

The effect of this scalar field is that the axial background field b is screened along the holographic direction. Since the holographic direction encodes the RG flow, we can define the analogue of a wave-function renormalization factor by

$$\sqrt{Z_A} b^{\mathrm{UV}} = b^{\mathrm{IR}} . \tag{44}$$

This implies that the axial Hall conductivity also suffers from this wave-function renormalization. Taking it into account one arrives at the prediction

$$\sigma^5_{\mathrm{AHE}} = \frac{Z_A}{3} \sigma_{\mathrm{AHE}} . \tag{45}$$

In other words the axial Hall conductivity is exactly $1/3$ of the electric Hall conductivity once the wave-function renormalisation of the axial gauge fields in IR is taken into account. This was investigated in ref. [40] and indeed found to be correct. Moreover since the prediction that the axial Hall conductivity is $1/3$ of the electric Hall conductivity is a fundamental property of the theory it should hold for all states. Again this can be checked by using the finite temperature backgrounds and indeed it is found that the relation holds exactly and independent of the temperature.

3.9 Disorder

Disorder is an integral component of any real condensed matter system. It is therefore not only interesting but also mandatory to study the effects of disorder even in semi-realistic models. In the case of the holographic Weyl semimetal, this has been initiated in ref. [66]. The authors study the effect of disorder in form of random Gaussian noise in the boundary value of the axial gauge field

$$\lim_{r\to\infty} A_z(r) = b_0 + 2\gamma \sum_{i=1}^{N-1} \sqrt{S(k_i)}\, \sqrt{\Delta k} \cos(k_i x + \delta_i) \tag{46}$$

with equally distributed momenta $k_i = \mathrm{i}k_0/N$, and random phases δ_i. The analysis is restricted to the so-called decoupling limit of holography in which the backreaction of the bulk matter fields on the AdS metric is neglected. Nevertheless the authors find rather interesting signatures of disorder on the quantum phase transition. In general the quantum phase transition is smeared due to the disorder. They also show the appearance of rare regions and indications of log-oscillatory structures in the Hall conductivity.

3.10 AC conductivities

The electrical AC conductivity in a holographic Weyl semimetal model was investigated in ref. [67]. A particularly interesting effect was pointed out in relation to the quantum critical behavior near the phase transition. On general grounds one expects the (zero temperature) optical conductivity to scale linearly with the frequency for low enough frequencies

$$\sigma(\omega) = c\omega . \tag{47}$$

This is simply enforced by the scaling symmetry of the Weyl fermions. The constant c is proportional to the number of active Weyl fermions. It was pointed out in ref. [67] that this can get modified for higher frequencies near the quantum phase transition. The frequency dependent optical conductivity enters then the quantum critical region whose scaling properties are determined by the scaling exponents of the Lifshitz critical point at the phase transition. The expected

change in scaling is

$$\sigma_{\parallel}(\omega) \propto \omega^{2-\beta}, \quad \sigma_{\perp} \propto \omega^{\beta}. \tag{48}$$

Most interestingly such a sudden change in frequency dependence of the optical conductivity at low temperature of the Weyl semimetal TaAs was experimentally observed in ref. [68]. The authors of ref. [67] suggest that this might be explained by assuming that one enters the quantum critical region in TaAs at a frequency around 30 meV. They find that a fit to the data gives a scaling exponent of $\beta = 0.14$ for the transverse conductivity in the Lifshitz quantum critical region. It should be noted that there are also other candidate explanations, such as activating of additional Weyl points at higher frequencies. Nevertheless the predicted change in scaling of the optical conductivity once the frequency is high enough to enter the quantum critical regime seems a robust prediction and is in principle accessible by experiments. It would be very interesting to see then if the scaling exponents of longitudinal and transverse optical conductivities can be fitted to weak coupling models or to predictions from holographic models.

3.11 Butterfly velocity

Holography has also contributed in recent years to the understanding of chaos in quantum many body systems. Quantum chaos can be characterized by the late time behavior of the out of time order correlation function (OTOC):

$$\langle [\mathcal{V}(t,\mathbf{x}), \mathcal{W}(0,0)]^2 \rangle \sim \mathrm{e}^{\lambda_{\mathrm{L}}(t-t^*-|\mathbf{x}|/v_{\mathrm{B}})}, \tag{49}$$

where λ_{L} is the Lyapunov exponent, t^* the so-called scrambling time and v_{B} the Butterfly velocity. The Lyapunov exponent obeys the bound [69]:

$$\lambda_{\mathrm{L}} \leq 2\pi T, \tag{50}$$

where T is the temperature of the system. It is saturated by holographic field theories. For a review on quantum chaos and holography see ref. [70]. Of particular interest is the behavior of the Butterfly velocity across a quantum phase transition. This question was addressed for the holographic Weyl semimetal model in ref. [71]. There the authors computed the Butterfly velocity in a holographic model with metric:

$$\mathrm{d}s^2 = -g_{tt}(r)\mathrm{d}t^2 + g_{rr}\mathrm{d}r^2 + h_{\perp}(r)\mathrm{d}\mathbf{x}_{\perp}^2 + h_{\parallel}(r)\mathrm{d}\mathbf{x}_{\parallel}^2. \tag{51}$$

This is precisely the metric that arises in the holographic Weyl semimetal where we chose $\mathbf{x}_{\parallel} = z$ and $\mathbf{x}_{\perp} = (x, y)$. The result can be seen in Figure 12.

It shows the surprising feature that the parallel component of the Butterfly velocity has a minimum whereas the perpendicular component shows a maximum at the quantum phase transition. The Butterfly velocity therefore does not show a universal behavior across the phase transition. This motivates the authors of ref. [71] to introduce a new quantity, the information screening length $L = 1/\mu$. It is defined as follows. First one introduces $M_\eta = \lambda_l / v_{\mathrm{B}}^{\eta}$ where $\eta \in \{\perp, \parallel\}$ and defines then

$$\mu^2 = \frac{1}{L^2} = \frac{M_\eta^2}{h_\eta(r_h)}. \tag{52}$$

This definition manages to get rid of the anisotropy such that a unique L independent of the direction can be defined. The authors show that L is maximal at the quantum critical point and they conjecture that the information screening length obeys

$$2L \leq \frac{1}{D_{\perp} + \beta D_{\parallel}} = 2L_c, \tag{53}$$

where β is the Lifshitz scaling exponent of the anisotropic directions, $D_{\perp}$ is the number of spatial dimensions with scaling exponent equal to one and $D_{\parallel}$ is the number of spatial directions with scaling β. They also point out that in holography the null energy condition restricts the scaling $\beta \leq 1$.

4 Weyl semimetal/Chern insulator transition

The phase diagram for Weyl semimetal is richer and it could go through a phase transition to a normal band insulator [31, 72] or to a Chern insulator [31, 73, 74] or to a metal [75] etc. However, the holographic Weyl semimetal model in sect. 3 goes through a quantum phase transition to a trivial semimetal phase in which only a part of degrees of freedom has been gapped out. This section reviews a holographic model describing a topologically nontrivial Weyl semimetal goes through a quantum phase transition to an insulating phase where all the degrees of freedom are gapped.

A generation of holographic Weyl semimetal model can be constructed as follows. We use the Stueckelberg trick to replace the complex scalar field Φ in eq. (11) by two real scalar fields ϕ and θ and introduce the general dilatonic couplings in front of the kinetic terms [76]:

$$\begin{aligned} S = \int \mathrm{d}^5x\sqrt{-g}\Big[& \frac{1}{2\kappa^2}\Big(R + 12 - \frac{1}{2}(\partial\phi)^2 - V(\phi)\Big) - \frac{Y(\phi)}{4}\mathcal{F}^2 \\ & - \frac{Z(\phi)}{4}(F)^2 + \frac{\alpha}{3}\epsilon^{abcde}A_a\Big(F_{bc}F_{de} + 3\mathcal{F}_{bc}\mathcal{F}_{de}\Big) \\ & - \frac{W(\phi)}{2}(A_a - \partial_a\theta)^2\Big]. \end{aligned} \tag{54}$$

Up to the anomaly the action eq. (54) is invariant under $\theta \to \theta + \chi$, $A_a \to A_a + \partial_a\chi$. One can show that the dual Ward identity for the conserved currents, which should be independent of the coupling strength of the system, is exactly the same as the one obtained from weakly coupled theory. The

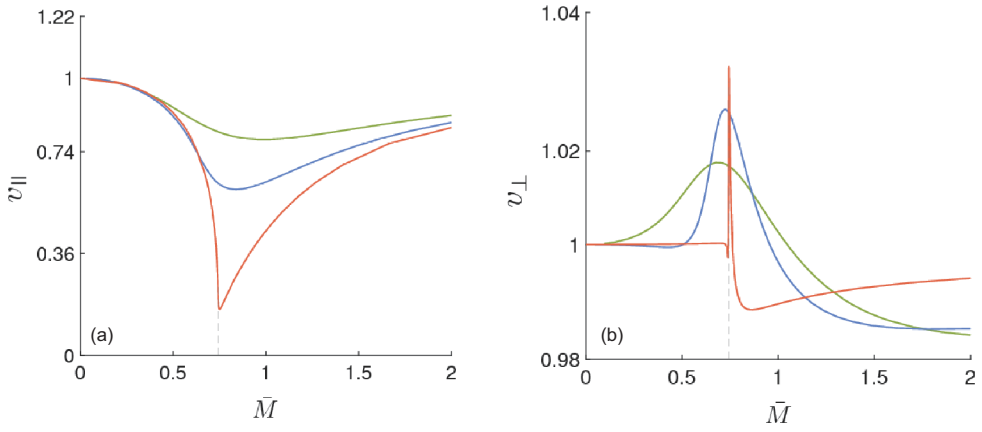

Figure 12 (Color online) Butterfly velocities as function of the dimensionless parameter $\bar{M} = M/b$ for different values of the temperature. (a) The parallel Butterfly velocity; (b) the perpendicular Butterfly velocity. As one can see the results are quite different, whereas the parallel one has a minimum, the perpendicular one develop a minimum. The lines show different temperatures $T/b = 0.005, 0.05, 0.1$ corresponding to the colors red, blue and green. Figures from ref. [71] CC BY 4.0.

holographic Weyl semimetal model in sect. 3 can be recovered via defining $\Phi = \frac{1}{\sqrt{2}}\phi e^{i\theta}$ which is axially charged under the axial gauge field and setting $Y(\phi) = Z(\phi) = 1$, $W(\phi) = q^2\phi^2$, $V(\phi) = \frac{m^2}{2}\phi^2$[9].

This section will focus on the physics at zero temperature. At $T = 0$ we use the same ansatz for the background fields as eq. (16) in sect. 3. To realise a holographic Weyl semimetal/insulator transition, the following dilatonic couplings are chosen:

$$Z(\phi) = 1\,, \quad W(\phi) = -q_0\left[1 - \cosh\left[\sqrt{\frac{2}{3}}\phi\right]\right], \qquad V(\phi) = \frac{9}{2}\left[1 - \cosh\left[\sqrt{\frac{2}{3}}\phi\right]\right], \tag{55}$$

and

$$Y(\phi) = \cosh\left[\sqrt{\frac{2}{3}}\phi\right]. \tag{56}$$

Note there is a Z_2 symmetry $\phi \to -\phi$ for eq. (54). When $\phi \to 0$, $W(\phi) \simeq \frac{q_0}{3}\phi^2$ and $V(\phi) \simeq -\frac{3}{2}\phi^2$. Thus q_0 plays a similar role as the axial charge. In the following we restrict to $q_0 > 0$. Near the conformal boundary, $\phi \to 0$, the potential in eq. (55) behaves as $V(\phi) = \frac{1}{2}m^2\phi^2 + \ldots$ with $m^2 = -3$. As already discussed in sect. 3, close to the boundary ($r \to \infty$) we have $\phi = \frac{M}{r} + \ldots, A_z = b + \ldots$.

At zero temperature, we first give the near horizon solutions. Similar to the holographic model in sect. 3, there are again three different kinds of near horizon geometries. Then we turn on irrelevant perturbations to get the full solutions.

Insulating phase The first kind of near horizon geometry is

$$u = r(1+r)\,, \quad h = r(1+r)\,, \quad A_z = a_1 r^{\frac{1}{4}(\sqrt{1+8q_0}-1)}\,, \qquad \phi = -\sqrt{\frac{3}{2}}\log\frac{r}{1+r}\,, \tag{57}$$

where a_1 is a free parameter which will make the geometry flow to AdS_5 with different value M/b. At the leading order, the geometry is known as the GPPZ gapped geometry [79]. Here we have a nontrivial A_z such that we will have an anisotropic geometry.

Weyl semimetal phase The second kind of geometry near the horizon is

$$u = r^2\,, \quad h = r^2\,, \quad A_z = a_0 + \frac{\phi_0^2}{4a_0 r}e^{-\frac{2a_0\sqrt{q_0}}{\sqrt{3}r}}\,, \qquad \phi = \frac{\phi_0}{r^{3/2}}e^{-\frac{a_0\sqrt{q_0}}{\sqrt{3}r}}\,. \tag{58}$$

At the leading order, the IR geometry is an AdS_5 with a constant A_z. a_0 can be rescaled to 1. The exponential terms play the role of the irrelevant perturbations. This near horizon geometry also shows up as the holographic Weyl semimetal phase in sect. 3.

Critical point The third kind of near horizon geometry is

$$u = u_0 r^2(1 + \delta u r^{\alpha_c})\,, \quad h = \frac{q_0}{9}r^{2\beta}(1 + \delta h r^{\alpha_c})\,, \tag{59}$$

$$A_z = r^\beta(1 + \delta a r^{\alpha_c})\,, \quad \phi = \sqrt{\frac{3}{2}}(\log\phi_1)\left(1 + \delta\phi r^{\alpha_c}\right). \tag{60}$$

In the case of $q_0 = 15$, we have $(u_0, \beta, \phi_1, \alpha_c) \simeq (1.150, 0.769, 1.797, 1.230)$ and $(\delta u, \delta h, \delta a) \simeq (0.147, -1.043, 0.591)\delta\phi$. At the leading order the system has a Lifshitz symmetry $(t, x, y, r^{-1}) \to c(t, x, y, r^{-1})$, $z \to c^\beta z$. We can use it to set

9) Studies on constructing insulating phases from generic holography with dilatonic coupling can be found in refs. [77, 78].

$\delta\phi = -1$. The irrelevant perturbations can flow the above geometry to AdS_5. In the boundary we get $(M/b)_c \simeq 0.986$. For arbitrary $q_0 > 0$, all the relevant perturbations around the above fixed point have complex scaling exponent, indicating that this fixed point is unstable [80, 81] which will be confirmed by studying the free energy.

The full solutions can be obtained by integrating the above near horizon geometries to the boundary. Different from the holographic semimetals in sect. 3, the near horizon behavior eq. (58) flows to AdS_5 with a nontrivial M/b that takes from zero to $(M/b)_{t+}$ with $(M/b)_{t+} > (M/b)_c$ and then decreasing to $(M/b)_c$. The near horizon geometry (57) flows to AdS_5 with M/b whose value is from infinity to $(M/b)_{t-}$ with $(M/b)_{t-} < (M/b)_c$ and then increasing to reach $(M/b)_c$ finally. Figure 13 shows the profiles of the matter fields at different M/b. Near the critical M/b, the matter fields shows oscillatory behavior (dashed color lines), which can be viewed as a sign of unstable critical solution.

With the bulk solution the free energy can be obtained numerically. Near the phase transition the behavior for free energy is shown in Figure 14. Different from the holographic model in sect. 3, for this holographic system at zero temperature there is a first order phase transition from the topologically nontrivial Weyl semimetal phase to an insulator phase. The different order of the quantum phase transition may indicate different underlying mechanisms for these two kinds of phase transitions. It can be easily checked that the phase transition is always of first order for any $q_0 > 0$.

The exact nature of the stable phases can be figured out by studying the conductivities. The real part of the optical longitudinal electric conductivity σ_{zz} of the holographic system at different M/b is shown in Figure 15. In the Weyl semimetal phase, σ_{zz} is linear in frequency at both small and large frequency regimes, which is quite similar to the discussion in sect. 3.10. There is a hard gap for σ_{zz} in the insulating phase, which indicates that it is indeed an insulating phase. Above the gap there is a continuous gapless spectrum and σ_{zz} eventually becomes also linear in frequency at large frequency. The width of the gap depends on M/b in a similar way comparing to the weakly coupled result, i.e. it monotonically increases when M/b increases and for sufficient large M/b, $\Delta/b \propto 0.22(M/b - 0.3)$.

The transverse conductivities can be calculated by considering fluctuations $\delta V_x = v_x(r)e^{-i\omega t}, \delta V_y = v_y(r)e^{-i\omega t}$. Define $v_\pm = v_x \pm i v_y$, from the holographic dictionary we can obtain the Green's functions $G_\pm$, from which we can compute G_{xx}, G_{yy} and G_{xy}. We have $\sigma_{xy} \pm i\sigma_{xx} = \pm\frac{G_\pm}{\omega}$, i.e.

$$\begin{aligned}\sigma_{\mathrm{T}} &= \sigma_{xx} = \sigma_{yy} = \frac{G_+ + G_-}{2i\omega}, \\ \sigma_{\mathrm{AH}} &= 8\alpha b - \sigma_{xy} = 8\alpha b - \frac{G_+ - G_-}{2\omega}.\end{aligned} \tag{61}$$

Figure 16 shows the full frequency dependence of transverse conductivities. Similar to the longitudinal conductivities, there is a gapless spectrum for $\mathrm{Re}[\sigma_{xx}(\omega)]$ and $\mathrm{Re}[\sigma_{yy}(\omega)]$ in the Weyl semimetal phase, while there exists a continuous gapless spectrum above a hard gap Δ/b in the insulating phase. The difference comparing to the longitudinal one is that if we increase M/b in the Weyl semimetal phase, $\mathrm{Re}[\sigma_{\mathrm{T}}]/\omega$ increases at small ω. Figure 16(b) shows the real part of optical anomalous Hall conductivity at different values of M/b. In the insulating phase at zero frequency the anomalous Hall conductivity goes to a nonzero value. Furthermore, the optical anomalous Hall conductivity has a smooth change at $\omega = \Delta$ in the insulating phase.

As already explained in sect. 3, the order parameter of the quantum phase transition is the DC anomalous Hall conductivity. In the topological phase, the DC conductivities can be analytically obtained $\sigma_{\mathrm{AHE}} = 8\alpha A_z(0), \sigma_{xx} = \sigma_{yy} = 0$. In the gapped phase, there is no simple analytical formula for σ_{AHE}. The DC anomalous Hall conductivity can only be calculated numerically by taking $\omega \to 0$ limit of $\mathrm{Re}[\sigma_{\mathrm{AH}}(\omega)]$, which is

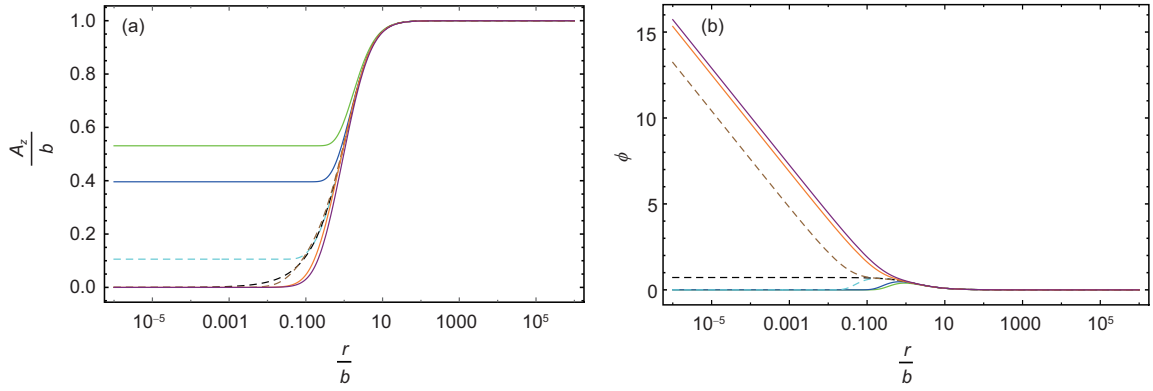

Figure 13 (Color online) The plots are for the profiles of A_z (a) and ϕ (b) at $M/b = 0.941$ (green), 0.983 (blue), 0.987 (dashed cyan), 0.986 (dashed black), 0.984 (dashed brown), 0.987 (orange), 1.019 (purple). The solid lines are for the stable phase while dashed lines are for the unstable phase. Figures from ref. [76].

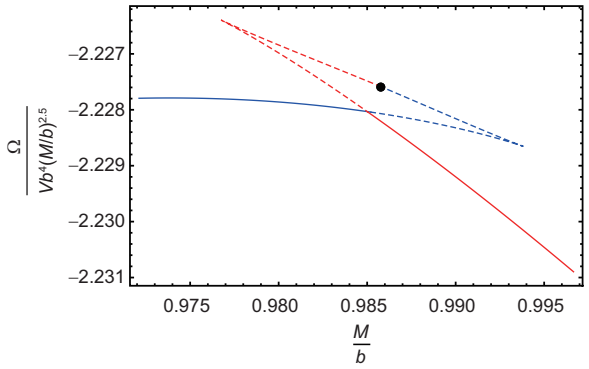

Figure 14 (Color online) This plot shows the free energy density. Here $q_0 = 15$. The blue (dashed) lines are for solutions from eq. (58) while the red (dashed) line are from eq. (57). The black dot is for the free energy at the unstable critical point. Figure from ref. [76].

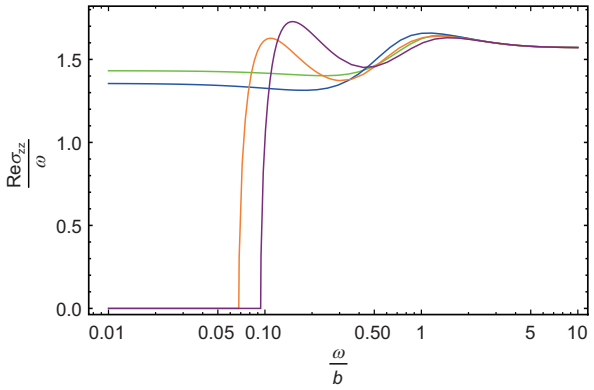

Figure 15 (Color online) The real part of optical longitudinal electric conductivity at $M/b = 0.941$ (green), 0.983 (blue), 0.987 (orange), 1.019 (purple). Figure from ref. [76].

different from the case for topological trivial semimetal in sect. 3.

Figure 17 shows the DC σ_{AHE} depending on M/b. When M/b increases, the anomalous Hall conductivity decreases and jumps at to another nonzero value. After the phase transition, σ_{AHE} looks insensitive to M/b. The discontinuity in σ_{AHE} indicates that the holographic quantum phase transition is indeed of first order. After the phase transition, in the diagonal components of the conductivities there exists a continuous gapless spectrum above a hard gap, whereas the DC σ_{AHE} is nonvanishing. These properties are exactly of a topological Chern insulator. Thus the holographic model introduced in this section describes a first order quantum phase transition from a strongly interacting topological Weyl semimetal to a topological Chern insulator.

From the field theoretical approach the phase diagrams for interacting Weyl semimetals have been studied in refs. [31, 72-74]. In ref. [72] it was found that for sufficiently strong interactions the Weyl semimetal can go through a first order quantum phase transition to a normal band insulator. The holographic model shows that the strongly interacting Weyl semimetal can also go through a first order quantum phase transition to a Chern insulator. Thus it reveals the intriguing phase structure for strongly correlated topological Weyl semimetal. The holographic model provides a novel framework to further explore the physics of strongly interacting topological states of matter.

5 Holographic nodal line semimetals

In addition to Weyl semimetals, there are several other examples of topological states of matter, including topological nodal line semimetal (NLSM), topological insulators, anomalous Hall states, topological superconductors and so on. In this section, we will focus on the physics of nodal line semimetals from holography.

In a NLSM [82] the shape of Fermi surface is a one dimensional circle in stead of nodal points in Weyl semimetals (see ref. [83] for a review). When it is topologically nontrivial, the system cannot be gapped by small perturbations unless going through a topological phase transition to another state.

5.1 Quantum field theoretical model

In Weyl semimetal, two Weyl points in the momentum space are separated at b while in nodal line semimetal there is a one dimensional circle of nodal line. Their low energy effective theories are also different. The Weyl semimetal is described by a Dirac field coupled to a time reversal symmetry breaking field, i.e. the axial gauge field A_z. Whereas for NLSM, it is described by a Dirac field coupled to a two form effective field $b_{\mu\nu}$ which breaks both time reversal and charge conjugate symmetry,

$$\mathcal{L} = -\mathrm{i}\bar{\psi}(\gamma^\mu\partial_\mu - m - \gamma^{\mu\nu}b_{\mu\nu})\psi, \tag{62}$$

where $\gamma^{\mu\nu} = \frac{\mathrm{i}}{2}[\gamma^\mu, \gamma^\nu]$ and $b_{\mu\nu} = -b_{\nu\mu}$ is an antisymmetric two form field. Note that we take the $(-,+,+,+)$ signature. Without loss of generality, a source of a two form b_{xy} is turned on. Then this system has the energy spectrum:

$$E_\pm = \pm\sqrt{k_z^2 + \left(2b_{xy} \pm \sqrt{m^2 + k_x^2 + k_y^2}\right)^2}. \tag{63}$$

The corresponding energy spectrum is shown in Figure 18. For $m^2 < 4b_{xy}^2$, the system is a topologically nontrivial nodal line semimetal with a circle nodal line of radius $\sqrt{4b_{xy}^2 - m^2}$[10]. For $m^2 > 4b_{xy}^2$, the system becomes an insulator and $m^2 = 4b_{xy}^2$ is the quantum phase transition point.

10) Note that the other components of $b_{\mu\nu}$ could also deform the nodal points to nodal line, e.g. nonzero b_{tz} would generate an accidental nodal line semimetal.

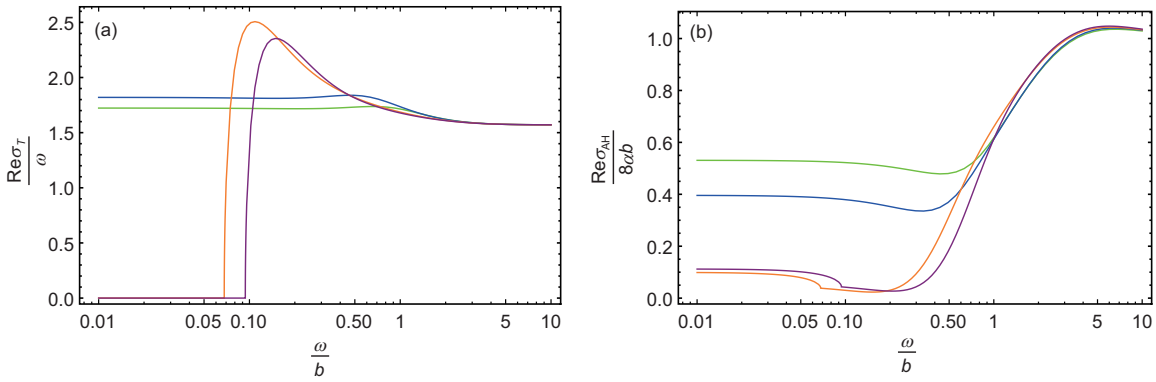

Figure 16 (Color online) The real part of the transverse optical electric conductivity (a) and the optical anomalous Hall conductivity (b) at $M/b = 0.941$ (green), 0.983 (blue), 0.987 (orange), 1.019 (purple) in the topological and the insulating phases. Figures from ref. [76].

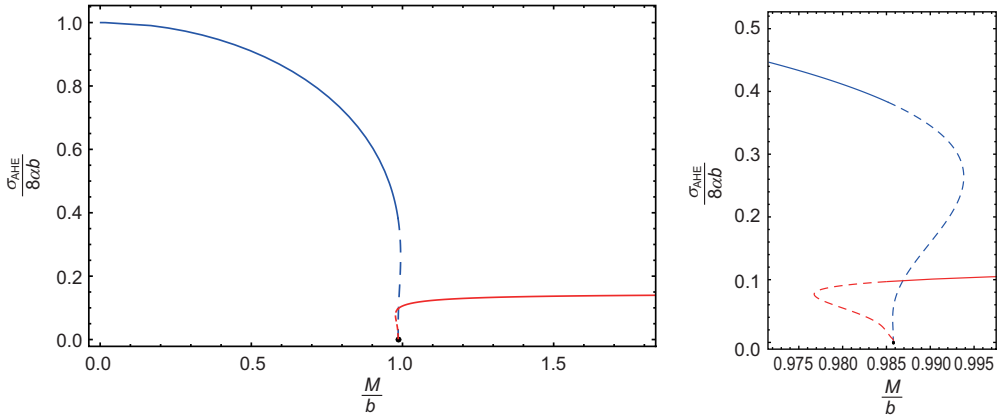

Figure 17 (Color online) Both plots are for σ_{AHE} at zero frequency and zero temperature from holography. The right plot is a zoomed in version of the left plot close to the quantum phase transition point. The solid and dashed lines are for stable and unstable phases separately. Figures from ref. [76].

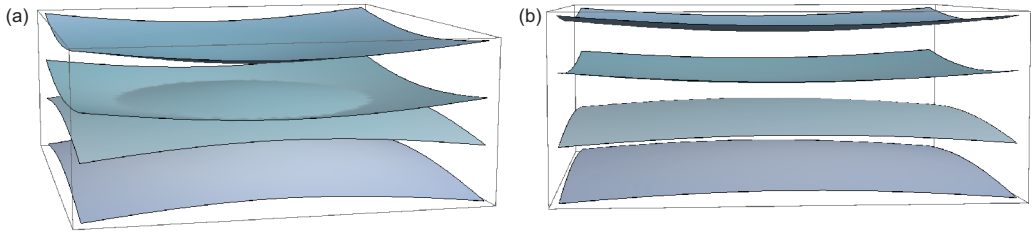

Figure 18 (Color online) The energy spectrum as a function of k_x, k_y for $k_z = 0$. (a) A nodal line appears at the band crossing when $m^2 < 4b_{xy}^2$; (b) for $m^2 > 4b_{xy}^2$ the system is gapped. Figures from ref. [84].

In the nodal line semimetal phase, close to the nodal line, the dispersion is linear in $\sqrt{k_x^2 + k_y^2} - \sqrt{4b_{xy}^2 - m^2}$ with velocity $\sqrt{1 - \frac{m^2}{4b_{xy}^2}}$ at $k_z = 0$ and linear in k_z with velocity 1 when $\sqrt{k_x^2 + k_y^2} = \sqrt{4b_{xy}^2 - m^2}$.

With a nontrivial background two form field $b_{\mu\nu}$, the electric current $J^\mu = \bar{\psi}\gamma^\mu\psi$ is still conserved while the axial current $J_5^\mu = \bar{\psi}\gamma^\mu\gamma^5\psi$ is no longer conserved. The following are the conservation equations:

$$\partial_\mu J^\mu = 0\,, \quad \partial_\mu J_5^\mu = -2m\bar{\psi}\gamma^5\psi - 2b_{\mu\nu}\bar{\psi}\gamma^{\mu\nu}\gamma^5\psi\,, \tag{64}$$

where anomaly terms have been ignored.

5.2 Holographic model

The NLSM model eq. (62) has shown that a coupling term $\bar{\psi}\gamma^{\mu\nu}\psi$ plays the role of deforming the single nodal point to a nodal loop. In holography we introduce on the gravity side a massive 2-form field B_{ab} which is dual to an antisymmetric tensor operator and is expected to play a similar role as the $\bar{\psi}\gamma^{\mu\nu}\psi$ operator. Similar to the holographic Weyl semimetal model, we also introduce an axially charged complex scalar

field Φ whose boundary value explicitly breaks the axial symmetry to generate the gap. The holographic NLSM can be realized from the following action [84]:

$$\begin{aligned} S = \int \mathrm{d}^5x\sqrt{-g}\Big[&\frac{1}{2\kappa^2}\Big(R+\frac{12}{L^2}\Big)-\frac{1}{4}\mathcal{F}^2-\frac{1}{4}F^2 \\ &+\frac{\alpha}{3}\epsilon^{abcde}A_a\Big(3\mathcal{F}_{bc}\mathcal{F}_{de}+F_{bc}F_{de}\Big) \\ &-(D_a\Phi)^*(D^a\Phi)-V_1(\Phi)-\frac{1}{3\eta}(\mathcal{D}_{[a}B_{bc]})^*(\mathcal{D}^{[a}B^{bc]}) \\ &-V_2(B_{ab})-\lambda|\Phi|^2B^*_{ab}B^{ab}\Big], \end{aligned}$$

where parts that do not involve B_{ab} are the same as the holographic Weyl semimetal (eq. (11)) in sect. 3. B_{ab} has to be axially charged since its dual operator's source explicitly breaks the axial symmetry. The potential terms in the action are

$$V_1 = m_1^2|\Phi|^2+\frac{\lambda_1}{2}|\Phi|^4\,,\quad V_2 = m_2^2B^*_{ab}B^{ab}\,, \tag{65}$$

where $m_{1,2}$ are mass of Φ and B_{ab}. Without loss of generality, B_{xy} component will be turned on in the following. In the following we set $q_1 = q_2 = 1, \lambda = \eta = 1, \lambda_1 = 0.1$ for simplicity.

Since the operators $\bar\psi\gamma^{\mu\nu}\psi$ and $\bar\psi\gamma^{\mu\nu}\gamma^5\psi$ are not independent, which indicates that there should be a self-duality in the real and imaginary part of the complex dual field B_{ab}, our strategy here is instead to consider a two form antisymmetric operator different from $\bar\psi\gamma^{\mu\nu}\psi$ and does not have the property of self duality. Note that some holographic QCD models [85, 86] considered the self-duality effect of the two form field.

We will focus again on the zero temperature physics and take the following ansatz:

$$\begin{aligned} &\mathrm{d}s^2 = u(-\mathrm{d}t^2+\mathrm{d}z^2)+\frac{\mathrm{d}r^2}{u}+f(\mathrm{d}x^2+\mathrm{d}y^2)\,, \\ &\Phi = \phi(r)\,,\quad B_{xy} = B(r)\,. \end{aligned} \tag{66}$$

Near the UV boundary $r\to\infty$, the expansions for the two matter fields $\phi(r)$ and $B(r)$ are

$$\phi = \frac{M}{r}+\cdots\,,\quad B = br+\cdots\,, \tag{67}$$

where M and b are the sources associated to the dual operators. At zero temperature, it turns out there are again three different kinds of near horizon geometries. Similar to the holographic Weyl semimetal, adding some irrelevant deformations, the near horizon geometries flow to an AdS_5 in the UV with some values of M/b.

Topological phase The first kind of near horizon geometry is

$$\begin{aligned} &u = \frac{1}{8}(11+3\sqrt{13})r^2\Big(1+\delta u\, r^{\alpha_1}\Big)\,, \\ &f = \sqrt{\frac{2\sqrt{13}}{3}-2}\,b_0r^\alpha\Big(1+\delta f\, r^{\alpha_1}\Big)\,, \\ &\phi = \phi_0r^\beta\,,\quad B = b_0r^\alpha\Big(1+\delta b\, r^{\alpha_1}\Big)\,, \end{aligned}$$

where $(\alpha,\beta,\alpha_1) = (0.183, 0.290, 1.273)$, $(\delta f, \delta b) = (-2.616, -0.302)\delta u$. We can further set b_0 to 1. At leading order there is a Lifshitz symmetry for the solution

$$(t, z, r^{-1})\to c(t, z, r^{-1})\,,\quad (x, y)\to c^{\alpha/2}(x, y)\,, \tag{68}$$

which can set $\delta u = \pm1$ where $\delta u = -1$ flows the geometry to AdS_5. Thus we have a unique free parameter ϕ_0 in the system.

It turns out we only get solutions with $M/b < 1.717$ in the UV. As ϕ_0 grows from 0, M/b also grows from the value 0 and becomes closer and closer to the critical value 1.717. From the property of holographic fermion spectral functions, one concludes the dual phase is a topological nodal line semimetal.

Critical point The second kind of near horizon geometry including irrelevant deformations is

$$\begin{aligned} &u = u_cr^2(1+\delta u\, r^{\beta_1})\,,\quad f = f_cr^{\alpha_c}(1+\delta f\, r^{\beta_1})\,, \\ &\phi = \phi_c(1+\delta\phi\, r^{\beta_1})\,,\quad B = b_cr^{\alpha_c}(1+\delta b\, r^{\beta_1})\,, \end{aligned}$$

with $(u_c, f_c, \alpha_c, \phi_c) \simeq (3.076, 0.828b_c, 0.292, 0.894)$, and $\beta_1 = 1.272\,, (\delta u, \delta f, \delta b) = (1.177, -2.771, -0.409)\delta\phi\,.$

We can set b_c to be 1. At the leading order there exists a same type of Lifshitz symmetry eq. (68) with a different scaling exponent α_c instead of α. This Lifshitz symmetry can set $\delta\phi$ to be -1 to flow to AdS_5 in UV. Therefore there is only one single such solution. We get the solution with the critical value $M/b \simeq 1.717$.

Trivial phase The third kinds of near horizon geometry is

$$\begin{aligned} &u = \Big(1+\frac{3}{8\lambda_1}\Big)r^2\,,\quad f = r^2\,, \\ &\phi = \sqrt{\frac{3}{\lambda_1}}+\phi_1r^{\frac{2\sqrt{160\lambda_1^2+84\lambda_1+9}}{3+8\lambda_1}-2}\,,\quad B = b_1r^2\sqrt{2}\sqrt{\frac{3\lambda+\lambda_1}{3+8\lambda_1}}\,. \end{aligned}$$

The ϕ_1- and b_1-terms above are the irrelevant deformations that flow the geometry to asymptotic AdS_5 solutions. In this case we only get solutions with $M/b > 1.717$.

Figure 19 shows the bulk profiles of matter fields ϕ and B/f at different M/b. Close to the critical M/b the IR solution flows quickly to the one for critical solution. The free energy of the system can be numerically studied and we find that when the phase transition occurs, the system is very continuous though the bulk IR solutions are discontinuous at the horizon. In holography this is a quite common feature for continuous quantum phase transitions.

5.3 A generic framework for topological states from hologrphy

This holographic nodal line semimetal has the same mathematical structure as the holographic Weyl semimetal in sect. 3. Ref. [84] proposed a general framework in holography to describe the strongly coupled gapless topological states. The bulk topological structure arises as follows.

- In the holographic system, there are at least two interacting matter fields. One of them dual to the operator which plays the role of mass effect, and the other dual to an operator which deforms the topology of the Fermi surface. For illustration these two fields are labeled as ϕ and A. The interaction between ϕ and A in deep IR generates interesting topological structure of the solution space.
- At zero temperature usually there exist three different kinds of solutions at the horizon. Two of them are the solution that at leading order A (or ϕ) is nonvanishing with $r^{-\delta_-^{A,\phi}}$ while at subleading order ϕ (or A) is sourced by A (or ϕ). There also exists a critical solution where both ϕ and A are subleading and sourcing each other. Because these two fields cannot be of leading order at the same time with $r^{-\delta_-^{A,\phi}}$ in IR, the semimetal phase cannot be gapped by small perturbations and is therefore topologically nontrivial.

The existence of a universal topological structure in the bulk suggests that in principle from holography we could obtain a large class of topologically nontrivial strongly coupled gapless systems.

5.4 Fermionic probe on the holographic nodal line semimetal

Although in NLSMs there is no sharp order parameter like anomalous Hall conductivity for Weyl semimetals, we could show that indeed there exists a circle of nodal loop in the dual fermionic spectral functions by probing fermions in the bulk.

Similar to the discussion for holographic Weyl semimetal in sect. 3.6, we utilize two spinors in the bulk to describe a Dirac operator in the dual field theory. In the bulk the coupling terms between the spinors and the scalar field are the same as the ones in the Weyl semimetal. There is one most natural way to couple the two bulk spinors to the two form field B_{ab}. We use the following action for the probe fermion:

$$S = S_1 + S_2 + S_{\rm int}\,, \tag{69}$$

$$S_1 = \int \mathrm{d}^5x\,\sqrt{-g}\mathrm{i}\bar{\Psi}_1\left(\Gamma^a D_a - m_f\right)\Psi_1\,,$$

$$S_2 = \int \mathrm{d}^5x\,\sqrt{-g}\mathrm{i}\bar{\Psi}_2\left(\Gamma^a D_a + m_f\right)\Psi_2\,,$$

$$S_{\rm int} = -\int d^5x\,\sqrt{-g}\left(\mathrm{i}\Phi\bar{\Psi}_1\Psi_2 + \mathrm{i}\Phi^*\bar{\Psi}_2\Psi_1 + \mathcal{L}_{\rm B}\right), \tag{70}$$

and

$$\mathcal{L}_{\rm B} = -\mathrm{i}(\eta_2 B_{ab}\bar{\Psi}_1\Gamma^{ab}\gamma^5\Psi_2 - \eta_2^* B_{ab}^*\bar{\Psi}_2\Gamma^{ab}\gamma^5\Psi_1)\,. \tag{71}$$

Note that in the bulk the Lorentz invariance in the tangent space has been explicitly broken.

The system has a rotation symmetry in the k_x-k_y plane and only depends on $k_{x-y} = \sqrt{k_x^2 + k_y^2}$. Without loss of generality we set $k_y = 0$. From the holographic dictionary, we can compute the retarded Green's function G. Then we could get its four eigenvalues and the spectral function. In the following we summarize the properties for the Green's function in the holographic nodal line semimetal.

- In all the three phases, for nonzero k_z, the retarded Green's function at zero frequency is real.
- In the trivial phase, the retarded Green's function is real for all values of $k_x, k_y, k_z \neq 0$. The pole is located at $k_x = k_y = k_z = 0$ and this is consistent with the explanation that this trivial semimetal phase is only partially gapped.
- For the critical point, among the four eigenvalues of the Green's function, two of them have peaks in the imaginary part at $k_x = k_y = 0$ and the other two are still small for all k_x, k_y.
- Figure 20 shows the spectral function $G^{-1}(0, k_x)$ for a finite regime of k_x at $k_z = \omega = 0$, $M/b \simeq 0.0013$ and $m_f = -1/4$. All the Green's function's four eigenvalues are

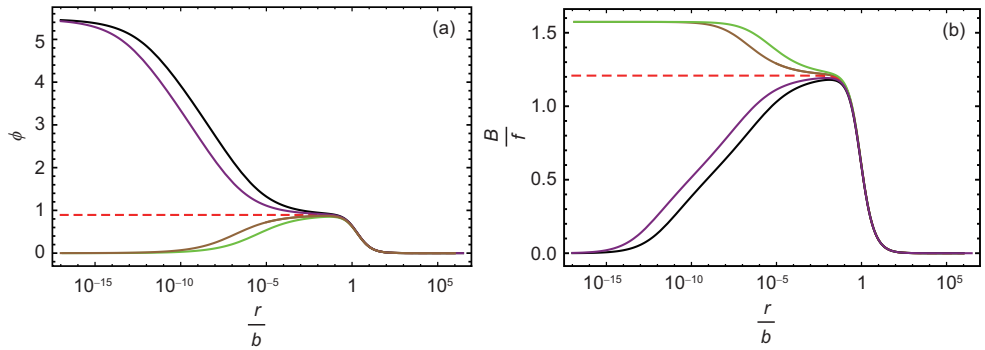

Figure 19 (Color online) The bulk profile for the scalar field ϕ (a) and the two form field B/f (b) for $M/b = 1.682$ (green), 1.702 (brown), 1.717 (red), 1.733 (purple), 1.750 (black). Figures from ref. [84].

real. They have the form $(g_1, -g_1, g_2, -g_2)$ with both g_1 and g_2 are positive and $g_1 \geq g_2$. The two eigenstates with eigenvalues $g_1, -g_1$ are labeled as "bands I" and the other two with $g_2, -g_2$ as "bands II". In Figure 20 different colors are used to distinguish different bands. Furthermore, since $-G^{-1}(0,k)$ can be treated as a topological Hamiltonian [43,45], the spectral density plot should qualitatively agree with the plot for eigenvalues in the ω-k_x plane.

- From Figure 20 we can see that between each two adjacent poles bands I and II always and only intersect once in the upper frequency plane. Between each two adjacent band crossing points there is always one pole and one zero of the Green's function.
- In the strongly coupled nodal line semimetal phase from holography there are multiple and discrete Fermi surfaces in the k_x-k_y plane at $k_{\mathrm{F}}^i = \sqrt{k_x^2 + k_y^2}$ and $k_z = 0, \omega \to 0$. The dual system has more complicated topological structure. At each nodal line momentum, there is a sharp peak (a pole at $\omega = 0$) in the imaginary part of two eigenvalues of the Green's function whereas the imaginary part of the other two is very small, which means that they are gapped.
- When k_x increases, the distance between adjacent poles becomes larger. At small k_x the poles are very close to each other. We have not plotted this regime in Figure 20 because the nodal loops are too dense to reveal all the poles and a much heavier numerics is required.
- When M/b increases, each nodal line momentum decreases and goes to zero at the transition point. Figure 21(a) shows the behavior of one k_{F}^i depending on M/b and Figure 21(b) shows the dispersion in the k_x direction at $M/b \simeq 0.0013$. Note that the dispersions in both the k_z and k_x directions are almost linear for each branch of nodal lines.

5.5 Topological invariants

In nodal line semimetals there are two kinds of topological invariants [83]. The first one is the Berry phase around a one dimensional closed line which links with the nodal loop in the momentum space. This one is related to the stability of the nodal loop under small perturbations in the system. The second one is the Berry flux around a sphere enclosing the whole nodal loop. This topological invariant is to describe whether the critical point is topological or not, which will not be discussed here.

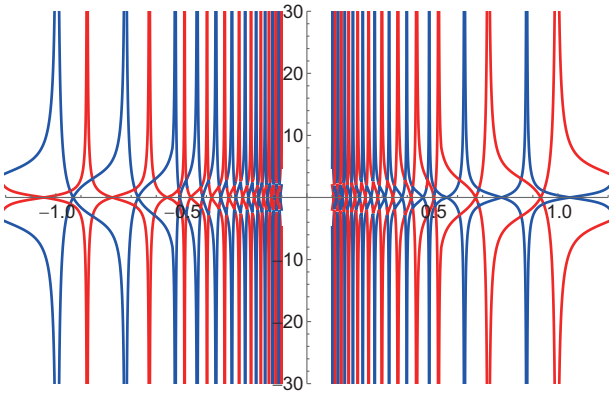

Figure 20 (Color online) Eigenvalues of $-G^{-1}(0,k_x)$ for $M/b \simeq 0.0013$. Red color is for bands I and blue color is for bands II. Figure from ref. [48].

From holography the strongly interacting NLSM phase has multiple while discrete nodal lines in the k_x-k_y plane and $k_z = 0$. Since the circle that links with two or more nodal lines at the same time can be continuously deformed to two or more separate circles each enclosing only one nodal line inside, we can focus on the Berry phase associated with each nodal line. From the Green's function at $\omega = 0$ we found that these poles are from two different sets of bands (bands I and II) which indicates that along the k_x axis the two gapped bands and two gapless bands exchange their roles alternatively. We could calculate the Berry phase numerically by choosing discrete points along the circle and found that there is a nontrivial Berry phase π associated with poles from band I and for poles from band II the Berry phase is undetermined. For the zeros of the Green's functions we have a trivial Berry phase of zero [48].

6 Alternative approaches

An approach to strongly coupled model of Weyl fermions based on holography that differs somewhat from the one reviewed in this article was presented in ref. [87]. There the idea is to study fermions which are strongly coupled in a holographic theory. This is similar to the study of probe fermions in holographic backgrounds [46,47]. The fermions are treated as probes which might or might not reflects the underlying physics of the dual field theory. It has been used for example to study the electric conductivity in ref. [88]. It would be interesting to explore the other characteristic features of Weyl semimetals including surface states, anomalous Hall effect etc., in this approach and to go beyond the probe limit to include the backreaction of the probe fermions to the gravitational background.

It is known that Weyl semimetals can also be generated from Dirac systems by applying a rotating electric field [89, 90]. More precisely the Dirac fermions split into left- and right-handed Weyl fermions under the application of a fast rotating electric field. The question if this also happens in holography has been investigated in ref. [91]. The construction is based on probe D7-branes in an $AdS_5 \times S^5$ background. The background serves also as energy reservoir and allows the formation of a non-equilibrium steady state. This

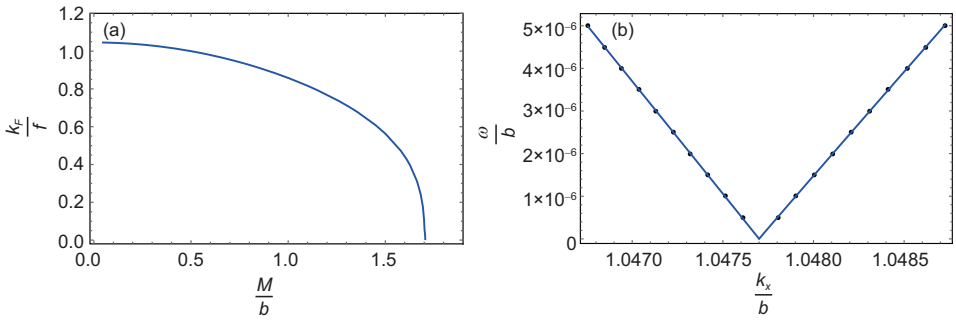

Figure 21 (Color online) (a) The nodal line momentum $k_F = \sqrt{k_x^2 + k_y^2}$ and $k_z = 0$. In both the critical and trivial phases, no Fermi surface exists at finite k whereas the pole is at $k = \omega = 0$ which is consistent with the fact that only partial degrees of freedom are gapped. (b) The dispersion relation associated to the nodal momenta in the left plot at $M/b \simeq 0.0013$. The best fit is for $k_x < k_F$, $\omega \simeq 0.005(1.0477 - k_x)^{0.998}$; while for $k_x > k_F$, $\omega \simeq 0.005(k_x - 1.0477)^{0.994}$. Figures from ref. [48].

allows to compute the Hall conductivity as function of the applied frequency of the driving electric field but also beyond the regime of linear response. In this top-down model the field content of the dual theory is clear, which in principle provides more constraints and insights into the physics of the boundary field theory. However, this model works in the probe brane limit while possible backreaction is not clear. It would be also interesting to explore more physics of the dual system from this approach.

7 Summary and outlook on further research

We have reviewed the holographic construction of models capable of reproducing key features of the physics of topological semimetals such as Weyl and nodal line semimetals. Amongst them the quantum phase transition to a topologically trivial state, the anomalous Hall conductivity, surface states, topological invariants, a new understanding of the axial Hall conductivity. Some of the new results derived from that model is the appearance of anomalous Hall viscosity in the quantum critical region at finite temperature of the phase transition. A short summary is given in Table 2 for Weyl semimetals and in Table 3 in the case of nodal line semimetals.

In these tables, we list different features of the weakly coupled semimetal and strongly coupled semimetal from holography for comparison, including the symmetries, transports/features, edge states, topological invariants and material realisation. In the nodal line semimetals, there is no sharp transport signature like anomalous Hall conductivity to distinguish the topological phase and trivial phase. The Fermi surfaces of the system show interesting features with nodal loop in the weakly coupled case and multiple loops in the strongly coupled case. The question marks are the items which are not clear yet.

So far only a small subset of the parameter space of these models has been explored. There are many open questions. An incomplete list is as follows.

- It would be interesting to include chemical potentials for vector and axial symmetries and study the chiral magnetic effect in these models. This would tell us about the CME in a strongly interacting Weyl semimetal. Meanwhile, it would be interesting to study negative magnetoresistivity in this model.
- In the quantum critical region a new anomaly related transport coefficient, anomaluos Hall viscosity appears. It would be interesting to develop the full hydrodynamics of the quantum critical region.
- The Weyl cones in Weyl semimetals can be tilted and so-called type II Weyl semimatals can appear if the tilt exceeds the "lightcone" defined by the Fermi velocity. Can one also construct holographic models of type II Weyl semimetals?
- The holographic Weyl semimetal in sect. 3 describes a holographic dual for Weyl semimetal with two Weyl nodes. It would be interesting to consider the holographic dual for multiple Weyl nodes.
- The quantum phase transition in the holographic WSM/Chern insulator model is of first order. It would be interesting to study if it is still first order for more general holographic phase transitions between Weyl semimetal and insulating phases.
- It would be interesting to explore the disorder effects or other momentum dissipation effects, finite temperature physics, transport physics etc., in the holographic WSM/Chern insulator model.
- The holographic insulating phase is a Chern insulator. It would be interesting to explore the topological invariants, to explore effects of surface states, to realise the phase transition to a normal insulator and so on.
- It would be interesting to construct the smoking gun transport in the holographic nodal line semimetals.
- In the holographic nodal line semimetal, it would be interesting to consider the holographic model with a self-dual

Table 2 The summary of holographic Weyl semimetal

Properties	Weakly coupled WSM	Holographic WSM
Symmetries	time reversal or inversion symmetry breaking	time reversal symmetry breaking
Transports	anomalous Hall conductivity	AHE , odd viscosity
Edge states	Fermi arc	surface current
Topological invariants	± 1	± 1
Material	TaAs, TaP, etc.	WP_2?

Table 3 The summary of holographic nodal line semimetal

Properties	Weakly coupled NLSM	Holographic NLSM
Symmetry	symmetry protected by mirror refection symmetry, inversion symmetry	symmetry protected by inversion symmetry
Features	nodal loop	multiple nodal loops
Edge states	no	?
Topological invariants	π	one set is π, another undetermined
Material	$PbTaSe_2$, ZrTe, etc.	?

two form field.

- It would be interesting to study the behavior of nonlocal quantities, e.g. entanglement entropy, Renyi entropy, complexity etc., across the topological phase transition, to characterize the changes of dynamical degrees of freedom during the transition.

These studies should be helpful in building holographic models for more complicated topological states of mater towards a classification of strongly interacting topological matter. We hope to explore some of these questions further in the future.

This work was supported by the National Key Research and Development Program of China (Grant No. 2018FYA0305800), and the Thousand Young Talents Program of China. The work of Yan Liu was also supported by the National Natural Science Foundation of China (Grant No. 11875083). The work of Ya-Wen Sun has also been partly supported by starting grants from University of Chinese Academy of Sciences and Chinese Academy of Sciences, the Key Research Program of Chinese Academy of Sciences (Grant No. XDPB08-1), and the Strategic Priority Research Program of Chinese Academy of Sciences (Grant No. XDB28000000). The work of Karl Landsteiner was supported by the MCIU/AEI/FEDER, UE (Grant Nos. SEV-2016-0597, FPA2015-65480-P, and PGC2018-095976-B-C21). We would like to thank Daniel Arean, Matteo Baggioli, Rong-Gen Cai, Alberto Cortijo, Chen Fang, Carlos Hoyos, Amadeo Jimenez, Eugenio Megías, Elias Kiritsis, Koenraad Schalm, Francisco Pena-Benitez, Maria Vozmediano, Zhong Wang, Jan Zaanen, FuChun Zhang for useful discussions and C. Copetti, J. Fernandez-Pendás, XuanTing Ji, Xin-Meng Wu and JunKun Zhao for enjoyable collaboration.

1 O. Vafek, and A. Vishwanath, Annu. Rev. Condens. Matter Phys. **5**, 83 (2014).
2 P. Hosur, and X. Qi, Compt. Rend. Phys. **14**, 857 (2013).
3 N. P. Armitage, E. J. Mele, and A. Vishwanath, Rev. Mod. Phys. **90**, 015001 (2018).
4 A. Vishwanath, Physics **8**, 84 (2015).
5 E. Witten, Riv. Nuovo Cim. **39**, 313 (2016).
6 J. S. Bell, and R. Jackiw, Nuov Cim A **60**, 47 (1969).
7 S. L. Adler, Phys. Rev. **177**, 2426 (1969).
8 D. T. Son, and N. Yamamoto, Phys. Rev. Lett. **109**, 181602 (2012).
9 J. Zaanen, Y. W. Sun, Y. Liu, and K. Schalm, *Holographic Duality in Condensed Matter Physics* (Cambridge University Press, Cambridge, 2015).
10 M. Ammon, and J. Erdmenger, *Gauge/Gravity Duality: Foundations and Applications* (Cambridge University Press, Cambridge, 2015).
11 S. A. Hartnoll, A. Lucas, and S. Sachdev, arXiv: 1612.07324.
12 J. Casalderrey-Solana, H. Liu, D. Mateos, K. Rajagopal, and U. A. Wiedemann, arXiv: 1101.0618.
13 R. G. Cai, L. Li, L. F. Li, and R. Q. Yang, Sci. China-Phys. Mech. Astron. **58**, 060401 (2015).
14 R. Baier, P. Romatschke, D. T. Son, A. O. Starinets, and M. A. Stephanov, J. High Energy Phys. **2008**, 100 (2008).
15 M. Rangamani, Class. Quantum Grav. **26**, 224003 (2009).
16 D. E. Kharzeev, Prog. Particle Nucl. Phys. **75**, 133 (2014).
17 K. Landsteiner, Acta Phys. Pol. B **47**, 2617 (2016).
18 J. Erdmenger, M. Haack, M. Kaminski, and A. Yarom, J. High Energy Phys. **2009**, 055 (2009).
19 N. Banerjee, J. Bhattacharya, S. Bhattacharyya, S. Dutta, R. Loganayagam, and P. Surówka, J. High Energ. Phys. **2011**, 94 (2011).
20 A. Gynther, K. Landsteiner, F. Pena-Benitez, and A. Rebhan, J. High Energ. Phys. **2011**, 110 (2011).
21 K. Landsteiner, E. Megías, and F. Pena-Benitez, Phys. Rev. Lett. **107**, 021601 (2011).
22 K. Landsteiner, E. Megías, L. Melgar, and F. Pena-Benitez, J. High Energ. Phys. **2011**, 121 (2011).
23 J. Gooth, F. Menges, N. Kumar, V. Sü, C. Shekhar, Y. Sun, U. Drechsler, R. Zierold, C. Felser, and B. Gotsmann, Nat. Commun. **9**, 4093 (2018).
24 J. Maldacena, Int. J. Theor. Phys. **38**, 1113 (1999); J. Maldacena, Adv. Theor. Math. Phys. **2**, 231 (1998).
25 I. R. Klebanov, and E. Witten, Nucl. Phys. B **556**, 89 (1999).
26 A. G. Grushin, Phys. Rev. D **86**, 045001 (2012).
27 A. G. Grushin, in *Common and not so common high-energy theory methods for condensed matter physics: Topological Matter, Springer Series in Solid-State Sciences, vol 190*, edited by D. Bercioux, J. Cayssol, M. Vergniory, and M. Reyes Calvo (Springer, Cham, 2018).
28 F. D. M. Haldane, Phys. Rev. Lett. **93**, 206602 (2004).
29 K. Y. Yang, Y. M. Lu, and Y. Ran, Phys. Rev. B **84**, 075129 (2011).
30 G. Xu, H. Weng, Z. Wang, X. Dai, and Z. Fang, Phys. Rev. Lett. **107**, 186806 (2011).
31 A. A. Burkov, and L. Balents, Phys. Rev. Lett. **107**, 127205 (2011).
32 A. A. Zyuzin, and A. A. Burkov, Phys. Rev. B **86**, 115133 (2012).

33 M. M. Vazifeh, and M. Franz, Phys. Rev. Lett. **111**, 027201 (2013).
34 F. D. M. Haldane, *Nobel lecture: topological phase transitions and topological phases of matter* (the Royal Swedish Academy of Sciences, 2016).
35 R. Jackiw, Int. J. Mod. Phys. B **14**, 2011 (2000).
36 P. Goswami, and S. Tewari, Phys. Rev. B **88**, 245107 (2013).
37 A. Jimenez-Alba, K. Landsteiner, Y. Liu, and Y. W. Sun, J. High Energ. Phys. **2015**, 117 (2015).
38 K. Landsteiner, and Y. Liu, Phys. Lett. B **753**, 453 (2016).
39 K. Landsteiner, Y. Liu, and Y. W. Sun, Phys. Rev. Lett. **116**, 081602 (2016).
40 C. Copetti, J. Fernández-Pendás, and K. Landsteiner, J. High Energ. Phys. **2017**, 138 (2017).
41 M. Heinrich, A. Jiménez-Alba, S. Moeckel, and M. Ammon, Phys. Rev. Lett. **118**, 201601 (2017).
42 M. V. Berry, Proc. R. Soc. A-Math. Phys. Eng. Sci. **392**, 45 (1984).
43 Z. Wang, and S. C. Zhang, Phys. Rev. X **4**, 011006 (2014); Z. Wang, and S. C. Zhang, Phys. Rev. X **2**, 031008 (2012).
44 Z. Wang, and B. Yan, J. Phys.-Condens. Matter **25**, 155601 (2013).
45 W. Witczak-Krempa, M. Knap, and D. Abanin, Phys. Rev. Lett. **113**, 136402 (2014).
46 H. Liu, J. McGreevy, and D. Vegh, Phys. Rev. D **83**, 065029 (2011).
47 M. Čubrović, J. Zaanen, and K. Schalm, Science **325**, 439 (2009).
48 Y. Liu, and Y. W. Sun, J. High Energ. Phys. **2018**, 189 (2018).
49 N. Iqbal, and H. Liu, Fortschr. Phys. **57**, 367 (2009).
50 G. Song, J. Rong, and S. J. Sin, J. High Energ. Phys. **2019**, 109 (2019).
51 H. B. Nielsen, and M. Ninomiya, Phys. Lett. B **130**, 389 (1983).
52 K. Landsteiner, Y. Liu, and Y. W. Sun, Phys. Rev. Lett. **117**, 081604 (2016).
53 E. M. Lifschityz, and L. P. Pitaevski, *Landau Lifschitz: Course of Theoretical Physics, Volume 10: Physical Kinetics* (Butterworth-Heinemann, Oxford, 1981).
54 J. E. Avron, R. Seiler, and P. G. Zograf, Phys. Rev. Lett. **75**, 697 (1995).
55 C. Hoyos, Int. J. Mod. Phys. B **28**, 1430007 (2014).
56 F. M. Haehl, R. Loganayagam, and M. Rangamani, J. High Energ. Phys. **2015**, 60 (2015).
57 A. Cortijo, Y. Ferreirós, K. Landsteiner, and M. A. H. Vozmediano, Phys. Rev. Lett. **115**, 177202 (2015).
58 P. K. Kovtun, D. T. Son, and A. O. Starinets, Phys. Rev. Lett. **94**, 111601 (2005).
59 A. Rebhan, and D. Steineder, Phys. Rev. Lett. **108**, 021601 (2012).
60 S. Jain, N. Kundu, K. Sen, A. Sinha, and S. P. Trivedi, J. High Energ. Phys. **2015**, 5 (2015).
61 C. Copetti, and K. Landsteiner, Phys. Rev. B **99**, 195146 (2019).
62 X. Ji, Y. Liu, and X. M. Wu, arXiv: 1904.08058.
63 A. Cortijo, D. Kharzeev, K. Landsteiner, and M. A. H. Vozmediano, Phys. Rev. B **94**, 241405 (2016).
64 D. I. Pikulin, A. Chen, and M. Franz, Phys. Rev. X **6**, 041021 (2016).
65 A. G. Grushin, J. W. F. Venderbos, A. Vishwanath, and R. Ilan, Phys. Rev. X **6**, 041046 (2016).
66 M. Ammon, M. Baggioli, A. Jiménez-Alba, and S. Moeckel, J. High Energ. Phys. **2018**, 68 (2018).
67 G. Grignani, A. Marini, F. Peña-Benitez, and S. Speziali, J. High Energ. Phys. **2017**, 125 (2017).
68 B. Xu, Y. M. Dai, L. X. Zhao, K. Wang, R. Yang, W. Zhang, J. Y. Liu, H. Xiao, G. F. Chen, A. J. Taylor, D. A. Yarotski, R. P. Prasankumar, and X. G. Qiu, Phys. Rev. B **93**, 121110 (2016).
69 J. Maldacena, S. H. Shenker, and D. Stanford, J. High Energ. Phys. **2016**, 106 (2016).
70 V. Jahnke, Adv. High Energy Phys. **2019**, 9632708 (2019).
71 M. Baggioli, B. Padhi, P. W. Phillips, and C. Setty, J. High Energ. Phys. **2018**, 49 (2018).
72 B. Roy, P. Goswami, and V. Juričić, Phys. Rev. B **95**, 201102 (2017).
73 C. Z. Chen, J. Song, H. Jiang, Q. Sun, Z. Wang, and X. C. Xie, Phys. Rev. Lett. **115**, 246603 (2015).
74 B. Roy, R. J. Slager, and V. Juričić, Phys. Rev. X **8**, 031076 (2018).
75 R. J. Slager, V. Juričić, and B. Roy, Phys. Rev. B **96**, 201401(R) (2017).
76 Y. Liu, and J. Zhao, J. High Energ. Phys. **2018**, 124 (2018).
77 E. Kiritsis, and J. Ren, J. High Energ. Phys. **2015**, 168 (2015).
78 C. Charmousis, B. Goutéraux, B. Soo Kim, E. Kiritsis, and R. Meyer, J. High Energ. Phys. **2010**, 151 (2010).
79 L. Girardello, M. Petrini, M. Porrati, and A. Zaffaroni, J. High Energy Phys. **1999**, 026 (1999).
80 S. A. Hartnoll, and L. Huijse, Class. Quantum Grav. **29**, 194001 (2012).
81 A. Donos, and S. A. Hartnoll, Nat. Phys. **9**, 649 (2013).
82 A. A. Burkov, M. D. Hook, and L. Balents, Phys. Rev. B **84**, 235126 (2011).
83 C. Fang, H. Weng, X. Dai, and Z. Fang, Chin. Phys. B **25**, 117106 (2016).
84 Y. Liu, and Y. W. Sun, J. High Energ. Phys. **2018**, 72 (2018).
85 G. E. Arutyunov, and S. A. Frolov, Phys. Lett. B **441**, 173 (1998).
86 R. Alvares, C. Hoyos, and A. Karch, Phys. Rev. D **84**, 095020 (2011).
87 U. Gürsoy, V. Jacobs, E. Plauschinn, H. Stoof, and S. Vandoren, J. High Energ. Phys. **2013**, 127 (2013).
88 V. P. J. Jacobs, S. J. G. Vandoren, and H. T. C. Stoof, Phys. Rev. B **90**, 045108 (2014).
89 X. X. Zhang, T. T. Ong, and N. Nagaosa, Phys. Rev. B **94**, 235137 (2016).
90 H. Hübener, M. A. Sentef, U. De Giovannini, A. F. Kemper, and A. Rubio, Nat. Commun. **8**, 13940 (2017).
91 K. Hashimoto, S. Kinoshita, K. Murata, and T. Oka, J. High Energ. Phys. **2017**, 127 (2017).